JCI insight

MMP2 and TLRs modulate immune responses in the tumor microenvironment

Luciana R. Muniz-Bongers, … , Miriam Merad, Nina Bhardwaj

JCI Insight. 2021. https://doi.org/10.1172/jci.insight.144913.

Research In-Press Preview **Immunology** **Oncology**

The presence of an immunosuppressive tumor microenvironment is a major obstacle in the success of cancer immunotherapies. Because extracellular matrix components can shape the microenvironment, we investigated the role of matrix metalloproteinase 2 (MMP2) in melanoma tumorigenesis. Significantly, we found that MMP2 signals pro-inflammatory pathways on antigen presenting cells which requires both toll-like receptor (TLR) 2 and TLR4. B16 melanoma cells that express MMP2 at baseline have slower kinetics in *Tlr2*$^{-/-}$*Tlr4*$^{-/-}$ mice, implicating MMP2 in promoting tumor growth. Indeed, *Mmp2* overexpression in B16 cells potentiated rapid tumor growth which was accompanied by reduced intra-tumoral cytolytic cells and increased M2 macrophages. In contrast, knockdown of *Mmp2* slowed tumor growth, and enhanced T cell proliferation and NK cell recruitment. Finally we found that these effects of MMP2 are mediated through dysfunctional dendritic cell (DC) - T cell cross-talk as they are lost in *Batf3*$^{-/-}$ and *Rag2*$^{-/-}$ mice, respectively. These findings provide insights into the detrimental role of endogenous alarmins like MMP2 in modulating immune responses in the tumor microenvironment.

MMP2 and TLRs modulate immune responses in the tumor microenvironment

Luciana R. Muniz-Bongers[1,2,†], Christopher B. McClain[1,2], Mansi Saxena[1,2], Gerold Bongers[1,3,†], Miriam Merad[1,3] and Nina Bhardwaj[1,2,4,*]

[1] Tisch Cancer Institute, Icahn School of Medicine at Mount Sinai, New York, NY, 10029, USA

[2] Hematology and Oncology Department, Icahn School of Medicine at Mount Sinai, New York, NY, 10029, USA

[3] Oncological Sciences Department, Icahn School of Medicine at Mount Sinai, New York, NY, 10029, USA

[4] Lead Contact

*Correspondence: nina.bhardwaj@mssm.edu; Icahn School of Medicine at Mount Sinai, Division of Hematology and Medical Oncology One Gustave L. Levy Place, Box 1079, New York, NY 10029-6574; Phone: 212-824-9358

[†]Current affiliation: Janssen Research and Development, LLC, Spring House, PA, 19103, USA

KEYWORDS

Tumor Microenvironment; Melanoma; Matrix Metalloproteinase 2; Toll-like Receptor 2; Toll-like Receptor 4

DECLARATION OF INTERESTS

Authors declare no competing interests.

ABSTRACT

The presence of an immunosuppressive tumor microenvironment is a major obstacle in the success of cancer immunotherapies. Because extracellular matrix components can shape the microenvironment, we investigated the role of matrix metalloproteinase 2 (MMP2) in melanoma tumorigenesis. Significantly, we found that MMP2 signals pro-inflammatory pathways on antigen presenting cells which requires both toll-like receptor (TLR) 2 and TLR4. B16 melanoma cells that express MMP2 at baseline have slower kinetics in *Tlr2*$^{-/-}$*Tlr4*$^{-/-}$ mice, implicating MMP2 in promoting tumor growth. Indeed, *Mmp2* overexpression in B16 cells potentiated rapid tumor growth which was accompanied by reduced intra-tumoral cytolytic cells and increased M2 macrophages. In contrast, knockdown of *Mmp2* slowed tumor growth, and enhanced T cell proliferation and NK cell recruitment. Finally we found that these effects of MMP2 are mediated through dysfunctional dendritic cell (DC) - T cell cross-talk as they are lost in *Batf3*$^{-/-}$ and *Rag2*$^{-/-}$ mice, respectively. These findings provide insights into the detrimental role of endogenous alarmins like MMP2 in modulating immune responses in the tumor microenvironment.

INTRODUCTION

The tumor microenvironment (TME) is a complex network of tumor and stromal cells, as well as signaling molecules that can dampen anti-tumor immune responses enabling tumor growth and maintenance. TME composition varies between tumor types, but broadly consists of angiogenic vascular cells, cancer-associated fibroblasts (CAFs), immune cells and an extracellular matrix that interact with tumor cells (1), (2). Matrix metalloproteinases (MMPs), a family of extracellular proteinases, are key components in promoting tumor progression through TME modulation. Many members of this family can cleave multiple ECM components and facilitate metastasis. Among these, MMP2 is overexpressed in many tumors, including melanoma, and high MMP2 levels in tumor or stromal cells is associated with increased tumor invasion and cancer progression, with patients often having poorer survival/prognosis (3). Elevated expression of some MMPs (such as MMP2, MMP1 and MMP13) has been directly correlated with poorer prognosis and MMP2 in particular has been associated with melanoma progression (4), (5), (6). Moreover, MMP2 has also been identified as a melanoma-associated antigen that is recognized by tumor infiltrating lymphocytes (TILs) (7), (8), (9), suggesting a dual role in promoting tumor growth but also in engaging anti-tumor immunity.

Initially the role of MMPs in tumorigenesis was presumed to be due to their proteolytic function, but they also have roles that are independent of their catalytic activity (10). In murine (m) macrophages, MMP-12 was shown to promote disruption of cellular membranes of phagocytosed bacteria in an enzymatically independent manner (11). Also, MMP14 modulates macrophage function in a protease-independent manner by regulating PI3Kδ signaling (12). We previously identified MMP2 as a cognate ligand for Toll-like receptor 2 (TLR2) signaling in human APCs that is independent of its catalytic activity. This interaction resulted in dendritic cell (DC) activation but skewing of T cells towards a T_H2 phenotype that is induced through TLR2 mediated OX40L expression and reduced IL-12 production (13). These observations highlight the

significance of TLR signaling in modulating immune responses that affect the TME. Indeed, several TLRs have been implicated in mediating pro- or anti-tumor activity in both tumor and immune cells in the TME (14), (15), (16), (17), (18).

Other endogenous TLR ligands, like high motility group box 1 (HMGB1), domain A of fibronectin, fibrinogen, β-defensin 2, soluble hyaluronan and heparan sulfate also modulate immunity via TLR activation on APCs in homeostasis and in the TME (19), (20), (21), (22), (23), (24). Versican (a matrix proteoglycan), is secreted by tumor cells and stimulates metastasis through TLR2 signaling in myeloid cells (25), (26). Similarly, Heat-shock protein 60 signals through TLR2 on tumor cells and promotes lung metastasis in mice (27). Intriguingly, including MMP2, all these molecules mainly target TLR2, 4 or 6, suggesting that activation of TLRs 2 and 4 via alarmins and subsequent modulation of cells in the TME may be an important process in tumorigenesis and even metastasis. TLR signaling on tumors is a double-edged sword and while some TLR agonists have shown anti-tumor effects, many studies reveal a role for TLR activation in promoting tumor growth (28), (14), (27), (29), (17). This duality might be tumor-specific where the TME composition influences TLR signaling, but it might also be due to the nature of the TLR ligand, subsequent downstream signaling pathways and consequent effects on immune cells.

With increasing evidence highlighting MMPs' role in tumor progression and metastasis, these factors are poised to be an attractive target for therapy. Inhibitors of MMPs have targeted many aspects of their biology, from the inhibition of their synthesis, their interaction with other proteins, to blocking their activity (30), however, synthetic MMP inhibitors (MPIs) failed in clinical trials to improve overall survival in patients with cancer possibly due to their lack of specificity (31), (32), (33). There is a need for selective inhibitors that can target individuals sets of MMPs in a specific tumor type, which could potentially improve clinical outcome in future trials, when used in combination with chemotherapy or immunotherapy approaches. For this, it is imperative to understand the diverse functions of MMPs, which in some cases may diverge from their canonical enzymatic activity.

Based on these observations, we speculated that MMP2 signaling via TLR2 might substantially impact tumorigenesis and metastasis thereby posing an attractive target for therapy. Interrogating the MMP2-TLR2 axis affords an opportunity to identify new and targeted therapeutic approaches to modulate anti-tumor immunity in vivo. In this study, we used murine models of cancer to dissect the effects of MMP2 in the regulation of immune responses in the TME.

RESULTS

MMP2 signals inflammatory responses through TLR2, TLR4 and MYD88

MMP2 modulates human DCs by TLR2 signaling and IFNAR1 degradation, modifying the DC cytokine response and subsequent T cell priming towards T_H2 cells (8). However, the precise mechanism by which MMP2 modulates anti-tumor immunity is still undefined. To shed light into this, we investigated MMP2's function in murine melanoma. To characterize the receptors involved in MMP2 signaling in murine APCs, we stimulated bone marrow (BM)-derived APCs with recombinant human (rh) MMP2 and assessed pro-inflammatory cytokine secretion. Control stimulants included MMP9 (MMP2's most related member) and TLR agonists Pam3CSK4 (TLR1/2), MALP2 (TLR2/6), LPS (TLR4), Poly I:C (TLR3) and R848 (TLR7). We previously ensured that our sources of MMPs were free of endotoxin contamination (8), (13). Primary BM-derived macrophages (BMDM) and DCs (BMDC) secreted TNFα and IL-6 (Figure 1A-B) in response to MMP2 but not to vehicle control or MMP9. As expected, the BMDMs and BMDCs secreted pro-inflammatory cytokines in response to the canonical TLR ligands (Pam3CSK4, MALP2, LPS, Poly I:C and R848), with only BMDCs lacking response to Poly I:C (Figure 1B).

Next, immortalized mouse bone marrow-derived macrophages (Im-Macs) lacking TLRs or downstream signaling adaptors (WT, *Tlr2*$^{-/-}$*Tlr9*$^{-/-}$, *Tlr4*$^{-/-}$, *Tlr2*$^{-/-}$*Tlr4*$^{-/-}$, *Myd88*$^{-/-}$, *Trif*$^{-/-}$*Myd88*$^{-/-}$, *Trif*$^{-/-}$ and *Tram*$^{-/-}$) were stimulated by TLR agonists and controls (Figure 1C and Figure S1). MMP2 required both TLR2 and 4 for signaling and cells that lacked either of these TLRs were significantly reduced in their ability to respond to MMP2 and secrete TNFα. Furthermore, TNFα secretion was almost completely abrogated in *Tlr2*$^{-/-}$*Tlr4*$^{-/-}$ Im-Macs (Figure 1C). In line with our previous published data (8), MMP2's enzymatic activity was dispensable as heat-inactivated (HI-MMP2) induced cytokine secretion in WT but not Tlr-deficient Im-Macs (Figure 1C). Notably, none of the cells responded to TLR3 stimulation by Poly I:C, indicating the lack of TLR3 expression upon BMDM immortalization (Figure S1A). MYD88 but not TRIF is involved in MMP2 signaling, as dual

Myd88$^{-/-}$ and *Trif*$^{-/-}$*Myd88*$^{-/-}$ cells but not *Trif*$^{-/-}$ cells lost their response to MMP2 as compared to WT cells (Figure S1B).

Since TLR2 and 4 were both necessary for MMP2 signaling, we evaluated the responsiveness of APC derived from double knock-out (DKO) *Tlr2*$^{-/-}$*Tlr4*$^{-/-}$ mice. CD11c^{+} DCs isolated from lungs and spleen of WT and DKO mice were stimulated with MMP2 or controls ex vivo. DCs from WT but not DKO mice responded to MMP2 by secreting pro-inflammatory cytokines (Figure 1D-E).

Finally, the physiologic relevance of MMP2 signaling via TLR2 and 4 in vivo was confirmed by injecting MMP2 and controls intraperitoneally in WT or TLR-deficient mice and assessing the pro-inflammatory cytokine response in the serum 3 hours later. TNFα secretion was evident in the serum of WT but not in *Tlr2*$^{-/-}$, *Tlr4*$^{-/-}$ or DKO mice (Figure 1F). Altogether, these data indicate that the signaling complex involved in MMP2 signaling in mAPCs is comprised of at least TLR2, TLR4 and MyD88 and is required for a response to MMP2 both in vitro and in vivo.

MMP2 binds to TLR2 and TLR4

To confirm that TLR2 and 4 interact with MMP2 and explore if other signaling mediators participate in the complex, we performed co-immunoprecipitation (coIP) experiments. HEK293T cells were co-transfected with murine *Mmp2* Flag and murine *Tlr2* HA or murine *Tlr4* Myc and, as shown previously (13), MMP2 bound and precipitated with TLR2. We also determined that TLR4 co-precipitated with MMP2 (Figure 2A). When all 3 plasmids were co-transfected, both TLR2 and 4 precipitated with MMP2, suggesting no competition for binding (Figure 2A). TLR2 and 4 binding was specific to MMP2 as they did not precipitate with MMP9 (Figure 2B) and MMP2 did not co-precipitate with mMyD88 (Figure 2B). To confirm specificity, we performed reverse IP by pulling down HA (TLR2) or Myc (TLR4) and probing for MMP2 (Figure 2C). Both TLR2 and 4, but not MYD88 bound MMP2. This suggests that TLR2 and 4 may form a heterodimer that binds to MMP2 and initiates a signaling complex that recruits MYD88 for signaling. Altogether, our data confirm

that MMP2 associates with TLR2 and 4 thereby accounting for the inflammatory responses seen in Figure 1.

MMP2 binds with TLR2 and TLR4 via its SP-Pro domains.

We next sought to identify which MMP2 domain binds the TLRs. Plasmids with different *Mmp2* domains expressing a Flag-tag (Figure 2D) were generated and coIP with full length *Tlr2*-HA was performed. The SP (signal peptide) and pro domains of the MMP2 protein were required for binding with TLR2 (Figure 2E). Using a plasmid expressing only SP + Pro domains we observed that they alone were sufficient for precipitation with TLR2 (Figure 2F). Due to technical difficulties, the constructs with only SP or only Pro domains could not be evaluated (Figure 2F).

Interestingly, the hemopexin domain which is involved in canonical roles of the MMP2 was dispensable for binding. Only when the hemopexin plasmid also included SP and Pro domains (*Mmp2*-PEX construct), was it able to precipitate TLR2 (Figure 2F). In summary, our data suggests that MMP2, through the presence of SP and Pro domains, binds TLR2 and 4 and forms a complex.

MMP2 expression in murine melanoma

We next evaluated MMP2 expression in melanoma using B16 F1 and F10 murine melanoma cells. We assessed MMP2 and TLR expression in 3 F1 cell lines (F1, F1 YFP-expressing, F1 OVA-expressing) and one B16 F10 line. MMP2 was detected in concentrated supernatants (Figure S2A) and in whole cell extract (WCE; Figure S2B) of all B16 cell lines tested. However, B16 cells lacked TLR2 expression by western blot (WB; Figure S2B). Upon stimulation with MMP2, MMP9 and TLR agonists (Pam3CSK4, MALP2, LPS, Poly I:C and R848) B16 F1 cell lines did not respond to MMP2 or any TLR agonists, whereas control BMDMs responded as expected (Figure S2C-D). Thus, while F1 tumor cells express MMP2 they lack the ability to

respond to TLR activation or MMP2 stimulation. These data exclude the possibility that autocrine or paracrine production of MMP2 will impact TLR2/4 dependent signaling pathways in tumor cells.

To determine if MMP2 is produced in B16 tumors in vivo, we sorted $CD45^+$, YFP^+ tumor and YFP^- stromal cells from tumors and evaluated gene expression by RT-PCR. *Mmp2* mRNA was expressed by both tumor and stromal cells, but not infiltrating $CD45^+$ cells (Figure S2E). YFP^+ tumor cells expressed neither *Tlr2* nor *Cd14* and expressed little *Tlr4*, indicating that in vivo they are also unlikely to signal upon TLR2-TLR4 ligation (Figure S2E and F). Altogether these data indicate that while our melanoma cells can produce MMP2, due to lack of signaling machinery they cannot directly respond to it in an autocrine or paracrine manner. However, MMP2 released by tumor cells may directly affect APCs or other cells within the TME that express *Tlr2* and 4.

Smaller tumor growth and kinetics in *Tlr2*$^{-/-}$/*Tlr4*$^{-/-}$ mice.

To determine whether *Tlr2* and 4 signaling is required for tumor progression, we monitored tumor incidence and growth up to 19 days following B16 F1 injection in WT, *Tlr2*$^{-/-}$, T*lr4*$^{-/-}$ and DKO mice. There was a significant delay in tumor growth with reduced tumor incidence and weight in DKO mice versus WT, while single *Tlr2*$^{-/-}$ and *Tlr4*$^{-/-}$ mice presented an intermediate phenotype (Figure 3A-C). Although the total number of cells isolated from DKO tumors was smaller, we observed no major differences in the percentage of immune cell infiltrates within total $CD45^+$ cells by FACS (Supplementary Figure 3A). Thus, the differences in tumor growth observed are likely due to differences in the quality or function of specific immune cell subsets rather than their quantity.

To gain a more comprehensive idea of the differences between WT and DKO, tumors were analyzed by CyTOF, using panels distinguishing lymphocytes or myeloid and stromal cells. 20 population clusters were identified on each panel (Figure 3D and E). The clusters could be separated between myeloid, lymphoid, stromal and tumor cell compartments based on distinct marker analysis and clustering (Figure 3F-G and S3B-C). Comparison between mouse WT vs

DKO mice was also performed to separate clusters differentially (Figure 3H-I). Statistically significant clusters were identified (Figure 3J-K and S3D-E). In the lymphocyte panel, we noted 5 clusters (#4, 5, 6, 12 and 16) which were statistically significantly decreased in tumors of DKO origin when compared to WT ones (Figure 3H and J). The clusters 4, 5, 6 and 12 include populations of T cells expressing CD4, CD39, CD73, KLRG1 and Ki67, all markers found to be expressed on regulatory T cells (34), (35). Cluster 16 includes a population of $CD25^+$ cells that express IFNγ, granzyme B and low levels of FoxP3, Ki67 and CD44. Based on these markers, this cluster might be composed of cytolytic T cells or a subset of NKT cells (36) (immgen.org). Altogether, we observed differences within the subpopulations in the T cell compartment in tumors of DKO mice that support the differences observed in the tumor growth (Figure 3G and S3).

With respect to myeloid cells, there was a significant decrease of 4 clusters in tumors from DKO mice as compared to WT, namely clusters #11, 16, 18 and 19 (Figure 3I and K). Based on marker expression (CD103, CD80. CD86, CD64, F4-80 and others), these cells were mainly composed of DCs, macrophages and granulocytes all sharing PD-L1 expression (Figure 3I and K). PDL1 expression by APCs in the TME and in the tumor draining LNs can inhibit T cell activation and can be detrimental for tumor growth (37) and the decrease of $PDL1^+$ myeloid cells observed in tumors from DKO mice might explain the slower tumor kinetics.

Finally, MMP2 expression was assessed by immunofluorescence (IF) staining of tumors from WT mice. MMP2-expressing cells were found proximal to $CD45^+$ cells (Figure 3L), suggesting an interaction between hematopoietic cells that express TLR2 and 4 and $MMP2^+$ tumor or stromal cells (13).

Altogether, these results indicate that the TME in DKO mice is characterized by a reduction in Treg-like cells and $PDL1^+$ APCs, suggesting a less immunosuppressive and immuno-exhaustive environment underlying the smaller tumor size and delayed kinetics.

Expression of TLR2 and TLR4 in the hematopoietic compartment aids tumor development.

We created bone marrow (BM) chimeras to dissect the role of TLR2 and 4 in stromal versus hematopoietic compartments for tumor growth. WT or DKO mice were sub-lethally irradiated and injected intravenously (i.v.) with WT or DKO BM cells (Figure S4A). There were no major differences in the ability of the BM cells to reconstitute blood (Figure S4B-C) or tissues such as lungs or spleen of WT mice (Figure S4D).

Following BM reconstitution, mice received B16 cells and tumor progression was monitored. Tumor growth and incidence was substantially reduced in WT mice with DKO BM as compared to ones with WT BM (Figure S4E-F). Donor BM, from WT and DKO origin, reconstituted recipients with the same efficiency and $CD45^+$ cells were found in tumors at similar proportions. However, because of smaller tumor sizes, the absolute number of reconstituted CD45.2 positive cells was lower in recipients receiving DKO BM (Figure S4G and data not shown). In complementary experiments, smaller tumors were observed in DKO recipients that received DKO BM when compared to WT BM, indicating a role for hematopoietic TLRs in modulating B16 tumor growth in vivo (Figure S4H). A role for non-hematopoietic cell TLR2 and 4 expression in supporting tumor growth was also noted, as tumors in DKO mice that received WT BM were smaller than the WT to WT controls and were similar in size as WT recipients that received DKO BM (Figure S4H).

Analysis of the TME by FACS did not reveal major differences in the proportion of recruited immune cell populations in any of the recipient groups (Figure S4I-J). No differences in IFNγ and TNFα single positive $CD4^+$ T cells were noted. However, there was a slight increase (although not significant) in the proportion of $IFN\gamma^+TNF\alpha^+$ $CD4^+$ T cells in tumors of WT mice that received DKO BM, when compared to WT BM (Figure S4K), suggesting a skewing towards T_H1 phenotype. These results indicate that the quality and function of the immune cell infiltrates in mice receiving DKO BM is altered and may account for the observed tumor growth differences. To confirm this, a more detailed dissection of the T cell quality, activation state and exhaustion phenotype of the T cells from these tumors will be needed.

In summary, the expression of *Tlr2* and *4* in the TME is important for the promotion of tumor growth, and when both of these receptors are absent, growth is compromised. Furthermore, the expression of *Tlr2* and *4* in both hematopoietic and stromal compartments appears to support *Mmp2*-driven tumor growth.

Overexpression of *Mmp2* in B16 cells accelerates tumor growth and promotes a pro-tumorigenic TME

The precise contribution of *Mmp2* in tumor cells was investigated through modulation of their MMP2 expression. First, *Mmp2* and *Mmp9* were stably overexpressed (O.E.) in B16 F1 cells (Figure S5A). The O.E. cells secreted active MMPs (Figure S5B) and had similar growth rates (Figure S5D) in vitro. In vivo, the *Mmp2* O.E. cells grew faster and bigger than the control tumors (Figure 4A). At days 18-20 tumor weight was measured (Figure 4B) and tumors were processed. IF confirmed the overexpression and distribution of MMP2 in the B16 O.E. tumors (Figure 4C) and displayed a pronounced recruitment of $CD45^+$ cells into the TME.

CyTOF was performed with lymphoid and myeloid/stromal cell panels. FlowSOM analysis revealed 20 population clusters (Figure S6A). Cells from *Mmp2* and *Mmp9* O.E. tumors clustered separately from each other (Figure S6B). Applying a graph-based clustering (tSNE), we identified clusters of lymphoid, myeloid and stromal/tumor origin (Figure 4D and G) based on the expression of single markers (Figure S6C and S6E). B cells, NK cells, $Foxp3^+$ T cells, $CD4^+$ T cell subsets and $CD8^+$ T cells were identified (Figure 4D and Figure S6C). The tSNE plots for the 3 different tumor groups: F1, F1 *Mmp2* O.E. and F1 *Mmp9* O.E. were generated (Figure 4E) to highlight the differential expression of the individual clusters (Figure S6D). A statistically significant decrease in 3 clusters was apparent when *Mmp2* O.E. tumor infiltrates were compared to WT infiltrates - #1, 11 and 12 (Figure 4F). Clusters 1 and 11 comprised of $CD8^+$ T cells positive for cytotoxicity marker Granzyme B and markers for activation and tissue resident memory (T_{RM}) or “stemness”, as recently described (38), (39). Based on the ectonucleotidase expression, e.g. CD39, these

could also be effector T cells differentiating towards exhaustion (40), (41), (42), (43), (44). Additionally, these $CD8^+$ T cells also expressed GITR, which while mostly known for its expression in T_{regs}, can also be expressed in activated $CD4^+$ and $CD8^+$ T cells, provide costimulation for $CD8^+$ T cell activation and promote $CD8^+$ T cell clonal expansion (45), (46), (47). Finally, cluster 12 included NK cells that express GITR and CD62L, indicating a possible mature polyfunctional NK cell population (48), (49) (Figure 4F and Figure S6D). Altogether *Mmp2* O.E. tumors appear to be selectively depleted of stem-like $CD8^+$ T cells and NK cells, both important for tumor control when activated. (50), (51), (52), (53).

With respect to myeloid cells, the tSNE plots for F1, F1 *Mmp2* O.E. and F1 *Mmp9* O.E. were generated (Figure 4H) to highlight the differential expression of the individual clusters (Figure S6E). 4 clusters were statistically different in *Mmp2* O.E. tumors versus controls- #1, 5, 7 and 15 (Figure 4I and S6F). Cluster 1 was increased in *Mmp2* O.E. tumors and comprised of cells high in CD44, low in MHCII, PD-L1 and Sca-1 (Ly6a) expression. Cluster 15, comprised of M2-like macrophages expressing CD11c, CD64, F4-80 and CD206, was also selectively increased in the *Mmp2* O.E. tumors. Two clusters were significantly smaller in *Mmp2* O.E. tumors, 5 and 7. Cluster 7 comprised of M1-like macrophages that express CD64, F4-80, MHCII and CX3CR1. Cluster 5 was characterized by $CD90.2^+$ $Sca1^+$ $CD45^+$, with lower levels of CD44, CD69 and CD86 expression, indicating they could be $CD8^+$ memory T cells or NKT cells (54), (55). Because the myeloid panel lacks CD4 or CD8, it is still unclear whether the cluster 5 comprised of CD4 or CD8 subsets.

These results were confirmed by IF where *Mmp2* O.E. tumors showed decreased granzyme B^+ cell infiltration (Figure 4J-K). Taken together, the results reveal that the TME of *Mmp2* overexpressing tumors in WT mice is enriched in M2-like macrophages but reduced in tumor-reactive cytotoxic $CD8^+$ T cells and polyfunctional mature NK infiltration, which together would compose a pro-tumorigenic TME.

Depletion of *Mmp2* in B16 cells reduces tumor growth and promotes T cell proliferation in the TME.

We next determined whether depleting tumors of *Mmp2* would alter growth kinetics. *Mmp2* knock out (KO) B16 cells were generated using the CRISPR-Cas9 RNP system and confirmed by a T7 endonuclease activity assay (Figure S5C). WT or *Mmp2* KO tumors grew at similar rates in vitro (Figure S5D). In vivo, however, *Mmp2* KO tumors were significantly smaller (Figure 5A) and had reduced weights (Figure 5B) when compared to WT tumors. Significant increases in immune populations with anti-tumor properties, such as $CD4^+CD25^-$ non-regulatory T cells, $CD103^+$ cross-presenting DC and M1-like Macrophages ($CD206^-$) were evident by FACS in the *Mmp2* KO tumors (Figure 5C). Additionally, a trend in increased NK cells and $PD\text{-}1^-$ $CD8^+$ T cells was observed. IF analysis confirmed the lack of MMP2 expression in *Mmp2* KO tumors growing in vivo (Figure 5D, lower panels). An increase in T cell proliferation shown by co-localization of CD3 and Ki67 (Figure 5E, white arrowheads) and higher levels of $CD8^+$ T cell infiltration were also confirmed in the *Mmp2* KO vs. WT tumors (Figure 5F-G). Finally, greater numbers of NK cells with associated Granzyme B infiltrated the tumor bed in *Mmp2* KO tumors. In contrast, NKs in WT controls localized mainly at the edges of the tumors (Figure 5H-I). The gating strategy for the flow cytometry is described in Figure S7. Altogether, the lack of *Mmp2* in F1 tumors promoted a higher tumor control and the immune landscape was characterized by T cell proliferation (indicated by Ki67 expression) and infiltration of cytotoxic T cells, NK cells, cross-presenting $CD103^+$ DCs and M1 macrophages.

The experiments with *Mmp2* O.E. and *Mmp2* KO tumors satisfactorily complement each other, indicating that *Mmp2* promotes immune dysregulation in the TME, by failing to recruit cytotoxic T cells or the cross-presenting $CD103^+$ DC and enhancing the infiltration of detrimental M2-like macrophages.

***Tlr2* and *Tlr4* are required for the accelerated growth of *Mmp2* overexpressing tumors**

To assess the role of host *Tlr2* and *4* in *Mmp2* O.E. and *Mmp2* KO tumor kinetics, we compared tumor growth in the *Tlr2*$^{-/-}$*Tlr4*$^{-/-}$ DKO mice. The accelerated growth of *Mmp2* O.E. tumors observed in WT recipients was lost in DKO recipients (Figure S8A) and tumors weights were similar (Figure S8B). There was, however, a higher tumor incidence in *Mmp2* O.E. tumors (Figure S8C). These results suggest that the rapid growth of *Mmp2* O.E. tumors relies on TLR2 and 4 expression in host cells. On the other hand, *Mmp2* KO tumors had impaired growth (Figure S8A) with smaller weights in DKO mice (Figure S8B). Overall, the incidence of *Mmp2* KO tumors was similar to WT controls but lower than *Mmp2* O.E. tumors in DKO hosts (Figure S8C).

FACS analysis of the TME of the DKO recipients revealed no major differences in the immune cell landscape between tumors from WT, O.E. or KO cells (Figure S8D-I). *Mmp2* overexpression in tumor cells is therefore likely to impact other pathways beyond *Tlr2/4* signaling that contribute to tumor growth, e.g. degradation of ECM proteins to modify the TME architecture or degradation of IFNAR1 in immune cells (APCs or other cell types) as we previously showed (8). Together, these results along with those in Figures 1 and 3 (and Figure S4), emphasize an important role for host derived *Tlr2* and *4* for potentiating tumor growth.

Accelerated tumor growth in *Mmp2* overexpressing cells partially depends on cDC1s and lymphoid cells.

Our studies identified a new mechanism by which *Mmp2* modulates anti-tumor activity: ligation of TLR2/4 on APCs promotes tumor infiltration of myelosuppressive populations while reducing tumor infiltrating CD4^{+} and CD8^{+} T cells, NK cells and CD103^{+} DCs. To firmly establish a role for DCs, we evaluated the growth of F1, *Mmp2* O.E. and *Mmp2* KO tumors in *Batf3*$^{-/-}$ mice which lack the cross-presenting cDC1 (56), including the CD103^{+} DCs (Figure 6A). In the absence of BATF3^{+} cells, the growth advantage of *Mmp2* O.E. tumors was lost. In contrast, *Mmp2* KO tumors showed significantly delayed growth (Figure 6A-B). These results support a role for BATF3^{+} DCs in *Mmp2* driven tumor growth but also suggest that non-BATF3^{+} APCs expressing

TLR2 and TLR4 also support tumor growth. Indeed, in mice both cDC1s (BATF3, $CD103^+$ subset) and cDC2s ($CD11b^+$ subset) express several TLRs, including TLR2 and 4 (57). FACS analysis did not reveal significant differences in the recruitment of immune cells into the TME (Figure 6C-D).

To evaluate the contribution of lymphoid cells towards *Mmp2* driven tumor growth, F1, F1 *Mmp2* O.E. and F1 *Mmp9* O.E. cells were injected into *Rag2*$^{-/-}$ mice which lack T and B cells (58) and tumor growth was monitored. Tumor size and growth patterns were comparable between different cell lines (Figure 6E-F). Analysis of the TME revealed no major differences in any immune cell infiltrates analyzed (Figure 6G). Altogether they indicate that *Mmp2* signals through both $BATF3^+$ DCs and T cells to enhance tumor growth and in the absence of *Mmp2* this dependency is lost.

We previously observed that MMP2 stimulated APCs prime T cells towards a T_H2 phenotype (13), which are typically detrimental towards tumor control (59), (60), (7). To determine whether MMP2 modulates its pro-tumorigenic effects through T cell skewing we activated OTII $CD4^+$ T cells (OVA-specific) and transferred them into *Rag2*$^{-/-}$ mice (i.v.). Two days later, we injected F1 cells that overexpressed OVA in the presence or absence of *Mmp2* (F1 OVA, F1 *Mmp2* O.E. OVA or F1 *Mmp2* KO OVA cells) and followed tumor growth kinetics. We theorized that MMP2 would skew T cells towards a T_H2 phenotype and potentiate tumor growth. Indeed, larger tumors were observed in *Rag2*$^{-/-}$ mice that received F1 *Mmp2* O.E. OVA cells vs. F1 OVA cells. Moreover, F1 *Mmp2* KO OVA tumors grew to a smaller degree than the other two cell lines (Figure 6H). Mice receiving F1 *Mmp2* O.E. OVA cells had higher mortality rates than mice receiving F1 OVA cells (Figure 6I). $CD45^+$ lymphocytes were isolated from tumors and stimulated in vitro with OTII peptide. Overall, $CD45^+$ cells from F1 *Mmp2* O.E. OVA tumors had higher levels of OX40L expression and increased fractions of IL-13^+ $CD4^+$ T cells, which correlates with a T_H2 phenotype (Figure 6J). Both F1 OVA and F1 *Mmp2* O.E. OVA tumors had more $CD25^+$ and PD-1^+ $CD4^+$ T cells than the F1 *Mmp2* KO OVA tumors. And in all 3 tumors, $CD4^+$ T cells were able

to proliferate at similar rates (shown by Ki67; Figure 6J). However, all the changes observed in Figure 6J are minimal and thus, a more in-depth phenotypic characterization (i.e. CyTOF or single-cell RNAseq) of the T_H subsets is necessary to indeed confirm a preference towards a T_H2-phenotype in the context if *Mmp2* overexpression.

In summary, *Mmp2* O.E. in melanoma cells promotes tumor growth and depends upon the presence of cDC1s and lymphocytes as the absence of either of these cell populations abrogates the growth advantages. Moreover, *Mmp2* O.E. skews priming of tumor antigen-specific T cells towards a T_H2 phenotype. These data align with our previous results in human cells in which MMP2 modulated APC priming of T cells towards a potentially pro-tumorigenic phenotype (13).

DISCUSSION

We previously identified several unique qualities of *MMP2* in human tumors. First, *MMP2* is a bona fide melanoma associated self-antigen that is recognized by both $CD4^+$ and $CD8^+$ T cells present in patient TILs, second, MMP2 is an alarmin that signals via TLR2 to activate human DCs and third, MMP2 primes T cells towards a deleterious T_H2 phenotype through the inhibition of IL-12 and induction of OX40L (9), (8), (13). In this context, overexpression of *MMP2* in melanoma would be predicted to have deleterious outcomes on the immune system, in addition to promoting tumor growth and invasion through modulation of the stromal architecture.

To address how *MMP2* mechanistically modulates tumor growth we adopted murine models of melanoma. We confirmed that the APC response to MMP2 stimulation requires *Tlr2* expression, but surprisingly also *Tlr4*, in a *Myd88* dependent manner. The involvement of both *Tlr2* and 4 in the response to MMP2 was confirmed in *Tlr2*$^{-/-}$*Tlr4*$^{-/-}$ mice. While the lack of both receptors completely abrogated the response to MMP2, a more modest phenotype was observed in either *Tlr2*$^{-/-}$ or *Tlr4*$^{-/-}$ mice, which could indicate a compensatory role of each TLR in the absence of the other.

CoIP experiments confirmed that MMP2 binds both TLR2 and 4 independently. MMP2 was shown to specifically and directly bind TLR2 in surface plasmon resonance experiments with high affinity (K_D=3.22 x 10^{-8} M) (13). Our coIP experiments, however, indicate that the MMP2-TLR4 interaction may not depend upon TLR2 as TLR4 precipitates with MMP2 even in the absence of TLR2. CD14, mostly known to mediate LPS transfer to a TLR4-MD-2 complex, but it was also shown to bind Pam_3CSK_4 (a TLR1/2 ligand) and direct it to TLR2 (61). Therefore, MMP2 binding to the TLR2-TLR4 complex might also rely on CD14 or other adaptors that are still unknown. Our data is also consistent with other reports that TLR2 and 4 form heterocomplexes and that MYD88 is critical for this heterodimer formation (62), (63), (64).

To dissect which domain of MMP2 binds to TLR2, we cloned different Flag-tagged *Mmp2* plasmids (Figure 2) and identified MMP2 SP and Pro domains as necessary for the binding. These

results are surprising as secreted MMP2 lacks the SP and Pro domains (cleaved off before secretion). One possibility is that in the context of tumors (like melanoma) the full length MMP2 protein might be secreted via exosomes from tumor or stromal cells. It is also possible that tumor cells release full length MMP2 as they undergo necrosis. Indeed, MMP2 (and other MMPs) has been found in exosomes derived from immune, tumor and stromal cells in the TME (65), (66), (67).

Since TLR2 and 4 can undergo internalization into endosomes upon activation, full-length MMP2 may also bind TLRs in this intracellular compartment. TLR4 internalizes into endosomes upon LPS stimulation (68), (69) and TLR2 can be internalized into endosomes via MyD88, TRAM and IRF7 or in a clathrin/dynamin dependent endocytosis process (70), (71), (72). MMP2 has been detected in endocytic membranes in association with calveolin proteins (73), (74). It can also associate with thrombospondin 2 and be taken up by low density lipoprotein-related receptor into endosomes similar to the endocytosis of MMP2-TIMP2 complexes (75), (76), (77). The non-canonical role of MMP2's SP-Pro domains in TLR2 signaling thus differs from MMP2's main role in degradation of ECM protein via its catalytic domain or in migration via its hemopexin domain (78). This could represent an additional way of regulating MMP2 activity in the context of tumor establishment and progression.

Since our results highlighted the requirement of TLRs in MMP2 signaling, we compared B16 growth in WT versus *Tlr2*$^{-/-}$*Tlr4*$^{-/-}$ DKO mice. We observed a significant delay in tumor growth and size in DKO mice, accompanied by changes in TME composition favoring a less regulatory environment. Our results corroborate other studies of tumor growth in *Tlr2* and *4* deficient mice, suggesting that *Tlr* deficiency mitigates tumor progression (25). Indeed, neutralization of TLRs in B16 melanoma with lung metastasis, Lewis Lung Carcinoma, and head and neck squamous cell carcinoma was shown to inhibit tumor growth and metastasis and tumor outcome (29), (79), (27).

Our B16 F1 cells lack TLR2 and 4 expression, ensuring that any response to MMP2 in the TME observed is due to host immune or stromal cells. The lack of TLR2 and 4 expression is not

unusual as B16 cells from different sources can vary in their expression of TLRs and adaptor molecules, with some groups reporting expression of TLR2, while others report the opposite (27), (14). BM chimera experiments, to distinguish the role of the hematopoietic vs. the non-hematopoietic compartment, indicated that TLR2 and 4 expression within the former was required for optimal tumor growth. Others have also shown that tumor derived TLR2 ligands (like versican) induced DC dysfunction in the B16 TME and in this context, lack of TLR2 or versican improved DC activation and subsequently T cell responses against the (26).

We confirmed a pro-tumorigenic role for MMP2 as its overexpression exacerbated tumor growth. *Mmp2* O.E. tumors had fewer infiltrating cytotoxic cells ($CD8^+$ T cells and NKs) and more M2-like macrophages. Additionally, there seemed to be a reduction in T_{RM} cells. T_{RM} have an important role in tumor control (both human and mouse tumors) and their presence is correlated with better clinical outcome (50), (51), (52), (53). Thus, the reduction of this population in *Mmp2* O.E. tumors highlights the detrimental role that overexpression of *Mmp2* has in the melanoma TME and explains the overt tumor growth.

In contrast, *Mmp2* KO tumors had slower growth kinetics and smaller size when compared to WT tumors. This was accompanied by an increase in $CD4^+$ and $CD8^+$ T cell, M1 like macrophages, NK cells and $CD103^+$ DC, with an increase in proliferating $CD4^+$ T cells ($Ki67^+$). This data is also consistent with patterns of delayed tumor growth in *Tlr2*$^{-/-}$ mice observed by others, suggesting that the disruption of detrimental TLR2-4 signaling in the tumor likely contributes to the control of tumor growth and restoration of immune cell function (26), (25). In a prostate cancer model using *Mmp2*$^{-/-}$ mice reduced liver metastasis and angiogenesis and increased survival was noted (80). We also observed an increase in $gp38^+$ stromal cells in *Mmp2* KO tumors. Gp38 is expressed by CAFs, stromal cells and $CD31^+$ endothelial cells. $Gp38^+$ stroma can serve as a barrier to prevent tumor cell invasion into the surrounding tissue and is correlated with improve prognosis (81). An increase in $CD31^+$ endothelial-like stromal cells was described in

other *Mmp2* deficient tumors suggesting their increased presence in *Mmp2*-deficient tumors contributes towards tumor control (82).

We investigated the role of relevant immune cell populations in controlling MMP2-driven tumor growth. BATF3 cDC1s ($CD8\alpha^+$ in lymphoid tissues and $CD103^+$ in non-lymphoid ones) were key in mediating MMP2 activity in tumors, as in their absence *Mmp2* O.E tumor growth was reduced. DC dysfunction due to TLR2 signaling in B16 melanoma has been previously described (26). Interestingly, *Mmp2* KO tumors also show a delay in growth kinetics in *Batf3*$^{-/-}$ mice when compared to B16 F1 controls. One possibility for this phenotype is that other DC subsets or APCs substitute for cDC1 activity in the absence of MMP2 and promote tumor control. Indeed, cDC2 are able to cross-present tumor antigens and induce $CD4^+$ T cell responses (including a T_H2 phenotype) not relying on BATF3 DCs (83), (84), (85), (86). It should be pointed out that *Batf3*$^{-/-}$ mice are not a perfect model for depletion of these cross-presenting DCs, as *Batf3* deficiency is not critical for $CD8\alpha^+$ DC generation (87), (88) or for cross-presentation to certain antigens to occur (89). Altogether, the effects in *Batf3*$^{-/-}$ mice highlight that cDC1s are negatively affected by overexpression of *Mmp2* and, in their absence, tumor growth in response to *Mmp2* overexpression is compromised.

The role for lymphocytes in mediating MMP2 modulatory effects was highlighted using *Rag* deficient mice. The absence of lymphocytes reduced the overt tumor growth of *Mmp2* O.E. cells and reconstitution with $CD4^+$ T cells ($OTII^+$) partially rescued the phenotype. Consistent with our previous data (13), *Mmp2* O.E. led to the skewing of tumor-specific T cells towards a T_H2 phenotype. Other groups have also shown similar associations between MMP2 and tumor progression and invasion (90), (3), (91).

In tumors overexpressing MMP2, we propose that tumor resident DCs and possibly other APCs such as TAMs, (92), are negatively modulated by MMP2 via their expression of TLR2 and 4. This in turn leads to skewed T cell priming, reduced CTL and NK cell activation and inefficient tumor control. Another possibility is that stromal cells, which can express TLR2 and 4 (92), are

similarly modulated by MMP2, indirectly affecting T cell responses, by acting on APCs or other immune cells. In this regard, stromal cells can produce inflammatory as well as immune suppressive factors. Signaling of TLR4 on mesenchymal stem cells in the TME, for instance, leads to suppression of NK cell cytotoxicity and MCP1 secretion, both associated with promotion of breast cancer cell migration (93).

Altogether, our results reveal complexities underlying MMP2 signaling in mice, in which TLR2, TLR4 and MYD88 are necessary. MMP2 expression in melanoma promotes tumor growth in a TLR2 and TLR4 dependent manner that requires APCs and T cells. These findings help pave the way for a potential new generation of MMP2 inhibitors, which could target the biding of MMP2 protein to TLRs and disrupt this deleterious MMP2 signaling in the context of tumors.

METHODS

Mice

WT C57BL/6J (#JAX:000664), CD45.1 (B6.SJL-*Ptprc*^{a} *Pepc*^{b}/BoyJ, #JAX:02014), TLR2$^{-/-}$ (B6.129-Tlr2^{tm1Kir}/J, #JAX:004650), TLR4$^{-/-}$ (B6.B10ScN-Tlr4$^{lps\text{-}del}$/JthJ, #JAX:007227), Rag2$^{-/-}$ (B6(Cg)-Rag2$^{tm.1Cgn}$/J, #JAX:008449) and OT-II (B6.Cg-Tg(TcraTcrb)425Cbn/J, #JAX:004194) mice were purchased from The Jackson Laboratory (www.jax.org). Tlr2$^{-/-}$Tlr4$^{-/-}$ mice were generated by crossing TLR2$^{-/-}$ and TLR4$^{-/-}$ mice. Batf3$^{-/-}$ (C.129S-Batf3^{tm1Kmm}/J, #JAX:013756) mice were obtained via Dr. Miriam Merad (Precision Immunology Institute and Tisch Cancer Institute, Icahn School of Medicine at Mount Sinai, New York, NY).

Cell lines and cell culture

Murine Im-Macs: Immortalized macrophages were used as previously described (94). Briefly macrophages were immortalized by infecting bone marrow progenitors with oncogenic v-myc/vraf expressing J2 retrovirus as previously described (95), (96) and differentiated into macrophages in media containing MCSF. Im-Macs were maintained in 10%FCS PSN DMEM (Gibco). Im-Macs lines have also been obtained from the BEI resources: TLR 3, 4, 7, 9, 2-9, 2-4, MYD88, TRIF, TRAM, TRIF- TRAM (BEI resources ATCC/NIAID; www.beiresources.org).

Primary BMDMs and BMDCs: BMDMs and BMDCs were generated from the bone marrow of 6–8-week-old female C57BL/6 mice. For BMDMs, cells were cultured in complete RPMI supplemented with 20ug/ml of murine colony stimulating factor (M-CSF, Prepotech #315-02) And for BMDCs, in complete IMDM supplemented with 200ng/ml of FMS-like tyrosine kinase 3 ligand (Flt3L, Prepotech #250-31L). Cells were cultured for 10 days, with media exchange on day 5.

B16 F1 cell lines: B16 F1 murine melanoma cell lines (ATCC #CRL-6326) and B16 F10 murine melanoma cell lines (ATCC #CRL-6475) were obtained from Dr. Miriam Merad (Precision

Immunology Institute and Tisch Cancer Institute, Icahn School of Medicine at Mount Sinai, New York, NY). Cells were maintained in complete RPMI media (as mentioned above). Cells were also IMPACT tested and were found free of contaminants and safe for in vivo injections into mice.

B16 F1 MMP-overexpressing cell generation: multisite gateway cloning system was used for lentiviral plasmid assembly and to overexpress *Mmp2* and *Mmp9* with a lentiviral plasmid using the EF-1α promoter. *Mmp2* and *Mmp9* inserts were cloned into an entry plasmid. Gibson HiFi assembly was performed to clone the purified inserts into the entry vector (EF-1α ENTR A plasmid). Multisite gateway LR recombination was performed using Invitrogen's Gateway LR Clonase II enzyme mix so that the inserts under the EF-1α promoter could be cloned into a destination vector containing puromycin resistance cassette (PuroR plasmid). Cells were co-transfected with *Mmp*-PuroR + GAG, VSV-G and Rev plasmids, viral supernatants were concentrated by ultra-centrifugation and transduced into B16 melanoma cells.

B16 F1 Mmp2 CRISPR knock out generation: 3 sgRNAs for mouse *Mmp2* and a pLentiCas9-EGFP plasmid were obtained from Genscript. sgRNA #3 and #5 were selected for Lentiviral generation. HEK293T cells were transfected with plasmids + Lentiviral packaging plasmids (Gag+Rev+VSV-G), using Lipofectamine 3000. Viral supernatant was concentrated by ultra-centrifugation. B16 F1 cells were transduced with pLentiCas9-EGFP and sorted based on GFP expression. Cas9-GFP^{high} cells were re-transduced with *Mmp2* sgRNA #3 or #5 lentivirus as described above. sgRNA expression selection was done by culture with puromycin. Mutation was confirmed with IDT's Surveyor Mutation Detection Kit and single cell clones were generated. The B16 F1 Cas9^{high} sg3 D1 clone was selected experiments, herein known as F1 *Mmp2* KO cells. F1 Cas9^{high} no sgRNA were used as controls.

Cell stimulation

Im-Macs, BMDCs and BMDMs were seeded in 96 flat-bottom well plates at 200,000 cells/well for primary cells and 100,000 cells/well for Im-Macs and stimulated with 5ug/ml rhMMP2 (Enzo Life Sciences), rh-MMP9 (EMD Millipore) or vehicle control (Enzo Life Sciences); 100ng/ml of Ultrapure LPS ; Pam3CSK4, MALP2 and R848 (all from Invivogen) and 2µg/ml HMW PolyI:C (Invivogen). Cells were stimulated for 16-20 hours for CBA and 8 hours for RT-PCR.

Cytometric Bead Array (CBA)

Supernatant from stimulated cells was collected and frozen at -20^{o}C until ready for use. CBA kits for mouse Inflammation (#552364) and mouse T_H1 and T_H2 cytokines (#551287) were purchased from BD Biosciences and the procedure was adapted from the manufacturer's directions. Analysis was done with the FCAP Software from BD Biosciences.

Transient transfection

HEK293T cells (ATCC #CRL-3216, RRID:CVCL_0063) were plated in 10cm plates and cultured overnight before transfection with 5ug of each plasmid, using Lipofectamine 3000 at a 1:2 ratio DNA:Lipofectamine in 1ml of Opti-MEM reduced serum media for 16-20 hours.

Western Blotting

Cells were collected in lysis buffer, incubated on ice for 30 minutes and centrifuged at 4^{o}C, 14000 rpm for 16 minutes. Protein quantification was performed using the Bradford assay. Lysates were separated as described before (13). Proteins were resolved by SDS/PAGE and transferred to PVDF membranes. Membranes were blocked, probed overnight with primary antibodies and incubated with secondary antibodies for 2 hours at RT. A complete list of primary and secondary antibodies used is in Supplemental table S1.

Plasmid design and preparation:

All plasmid constructs were designed in the laboratory by L.R.M.B. and generated by Genscript (www.genscript.com). *Mmp2*-Flag tagged and all MMP2 domains + Flag tags were generated based on codon-optimized full length murine *Mmp2* sequence. Murine *Tlr2*-HA and murine *Tlr4*-Myc constructs were also codon optimized. The *Mmp2*-Pex (PEX-LV) construct was a gift from Inder Verma (Addgene plasmid #12120) (97).

Co-immunoprecipitation

200µg of protein lysate was used for co-immunoprecipitation. Protein was incubated with anti-FLAG M2 magnetic beads, Monoclonal anti-HA agarose antibody or Anti-c-MYC Agarose Affinity gel antibody overnight. For immunoprecipitation, samples were eluted using 3x FLAG peptide, HA peptides or c-MYC peptide. Samples were further analyzed using western blotting.

Bone-marrow (BM) chimeras

BM isolation: Tibia and femurs of donor mice were collected. Bone tips were cut and and BM flushed using a 27G needle and RPMI into 50ml tubes with a 70µm strainer. Cells were centrifuged and incubated with ACK lysis buffer for red blood cell lysis.

Irradiation and BM injections: mice were irradiated with 2 doses of 600 rads (6Gy), 4 hours apart. 100ul ($4x10^6$ cells) of cell suspension was injected into the tail vein. 6-8 weeks post BM transfers, blood was collected, lysed of red blood cells and stained with an antibody cocktail mix for 30 minutes. FACS was performed to check CD45.1 versus CD45.2 engraftment.

Tumor processing

Tumors were collected between days 15-21 post-injections and dissociated using the mouse tumor dissociation kit (130-096-730) and gentleMACS from Miltenyi Biotec, using program 37°C_m_TDK1. Macerated tumors were passed through a 70µm cell strainer, washed with RPMI and centrifuged at 300g, 8 min, 4°C. Cell pellets were ressuspended in 2 ml of ACK lysis buffer

for 2 minutes, at RT and washed in 1x PBS (300g, 8 min, 4°C). Single cell suspension was analyzed by FACS or CyTOF.

FACS analysis of TILs

Single cell suspensions were aliquoted into round-bottom 96-well plates, ressuspended in 100-150µl of antibody mixes and incubated at 4°C, 30 minutes, in the dark. For ICS, samples were processed with eBiosciences FoxP3 Staining Kit (as per manufacturer's instructions) and incubated in 150µl of ICS Ab mix at 4°C, 30 minutes. Antibodies used are listed in Supplemental table S2.

Cytometry by Time of Flight (CyTOF)

3-5 x 10^6 live cells were taken for CyTOF at the Human Immune Monitoring Core facility of the Tisch Cancer Institute, Icahn School of Medicine at Mount Sinai (https://icahn.mssm.edu/research/human-immune-monitoring-center), where they were prepared for CyTOF as per the facility protocol. One lymphoid and one myeloid panel were designed, and samples were analyzed based on these. Antibodies panel and metal conjugations were generated and optimized by the Human Immune Monitoring Core facility. Supplemental table S3 contains the complete list of metal-conjugated antibodies.

CyTOF analysis

Analysis was performed using R software. Barcoded FCS files were read and transformed using a hyperbolic inverse sine (asinh) with a cofactor of 5 using R/Bioconductor/flowCore 1.48.1 (B Ellis, Perry Haaland, Florian Hahne, Nathan Le Meur, Nishant Gopalakrishnan, Josef Spidlen, Mike Jiang and Greg Finak (2019). flowCore: flowCore: Basic structures for flow cytometry data.). Cell counts were between 196K and 558K. Unsupervised multi-dimensional scaling (MDS) plots were generated using R/Bioconductor/limma 3.38.3 (Ritchie, M.E., Phipson, B., Wu, D., Hu, Y.,

Law, C.W., Shi, W., and Smyth, G.K.). Hierarchical clustering with Euclidean distances was performed using R/Bioconductor/FlowSOM 1.14.1 and R/Bioconductor/ConsensusClusterPlus with a maximum of 25 clusters. t-stochastic neighbor embedding (t-SNE) (Van Der Maaten and Hinton. Visualizing data using t-SNE. JMLR, 2008) was calculated using R/CRAN/Rtsne 0.15. Statistical analysis was performed using binomial generalized linear mixed-effects model (GLMM) from the R/CRAN/lme4 1.1-20 package, p values were adjusted using FDR. Heatmaps were generated with R/CRAN/pheatmap 1.0.12 and all other plots were generated using R/CRAN/ggplot2 3.1.0.

B16 tumors fixation, freezing and sectioning

B16 melanomas were collected and incubated in Periodate-Lysin-Paraformaldehyde (PLP) solution overnight at 4°C. Tissues were then washed in a sodium phosphate buffer (mixture of sodium phosphate monobasic and dibasic buffers) for 1-3 minutes and dehydrated by successive sucrose gradients (10%, 20% and 30%), each for 2 hours at 4°C. They were then embedded in OCT, frozen and kept in -80°C. Using a cryostat, 7-10µm sections were cut and transferred into superfrost slides and kept at -20°C.

Immunofluorescence of frozen sections

Frozen slides were permeabilized with 1x TBS + 0.1% Triton-X for 15min at RT, then washed with 1x TBS. Tissues were blocked with 10% BSA/TBS for 15-20min at RT and slides were incubated with primary antibodies overnight at 4°C. Slides were washed for 10min in TBS, RT and incubated with secondary antibodies at RT, dark for 2 hours. Slides were washed twice in 1x TBS and then mounted using ProLong Antifade Reagent with DAPI (Thermo Fisher Scientific, #P36931). Supplemental table S4 includes a list of antibodies used.

Statistics

For all graphical analyses, mean values and S.E.M values were displayed. Student's t- test (two-tailed, unpaired), one-way or two-way ANOVA with Dunnet's post hoc test, Multiple unpaired T-test with using Holm-Sidak correction for multiple comparisons were calculated using Prism 8 (GraphPad). A P value less than 0.05 was considered significant.

Study Approval

All experimental procedures using mice were approved by the Institutional Animal Care and Use Committee of the Icahn School of Medicine at Mount Sinai and were conducted in accordance with institutionally approved protocols and guidelines for animal care and use.

AUTHORS CONTRIBUTIONS

L.R.M.B. designed and conducted the experiments, data analysis and drafted the manuscript. C.B.M. assisted with tumor collection and processing experiments and generated some of the lentiviruses used in the B16 transduction experiments. G.B. performed CyTOF and RNAseq analysis. L.R.M.B, M.S. and N.B. interpreted and discussed the data. M.M. provided some mouse lines and gave insight on experiment planning and data discussion. N.B. supervised experiment designs, developed the manuscript and secured funding for the project.

ACKNOWLEDGEMENTS

This work was supported by the National Institutes of Health, United States grant RO1CA180913 (to N.B.), the Melanoma Research Alliance grant TSA #412518 (to N.B.), The Kimberly and Eric J. Waldman Department of Dermatology at the Icahn School of Medicine at Mount Sinai and by the 2015 Peer Reviewed Cancer Research Program Horizon Award from Department of Defense Office of the Congressionally Directed Medical Research Programs (CDMRP) GRANT12001223 (to L.R.M.B.). We thank Adiel Munk, MD for maintaining the mouse immortalized cells; Jenna Newman, PhD for assistance in editing the manuscript; Sreekumar Balan, PhD for assistance with DC subsets identification and isolation; and Antoine Tanne, PhD for obtaining the Im-Macs cell lines. We thank Linda Hammerich, PhD for assistance in tail vein injections. We also thank the Mount Sinai Human Immune Monitoring Center (HIMC), Adeeb Rahman, PhD and specially Brian Lee, for help in planning and antibody panel design and sample processing by CyTOF.

REFERENCES

1. Hanahan D, Coussens LM. Accessories to the crime: functions of cells recruited to the tumor microenvironment. *Cancer Cell*. Mar 20 2012;21(3):309-22. doi:10.1016/j.ccr.2012.02.022
2. Wu T, Dai Y. Tumor microenvironment and therapeutic response. *Cancer Lett*. Feb 28 2017;387:61-68. doi:10.1016/j.canlet.2016.01.043
3. Hofmann UB, et al. Matrix metalloproteinases in human melanoma. *J Invest Dermatol*. Sep 2000;115(3):337-44. doi:10.1046/j.1523-1747.2000.00068.x
4. Airola K, et al. Expression of collagenases-1 and -3 and their inhibitors TIMP-1 and -3 correlates with the level of invasion in malignant melanomas. *British Journal of Cancer*. May 1999;80(5-6):733-743. doi:DOI 10.1038/sj.bjc.6690417
5. Vaisanen A, et al. Prognostic value of MMP-2 immunoreactive protein (72 kD type IV collagenase) in primary skin melanoma. *J Pathol*. Sep 1998;186(1):51-8. doi:10.1002/(SICI)1096-9896(199809)186:1<51::AID-PATH131>3.0.CO;2-P
6. Kurschat P, et al. Identification of activated matrix metalloproteinase-2 (MMP-2) as the main gelatinolytic enzyme in malignant melanoma by in situ zymography. *J Pathol*. Jun 2002;197(2):179-87. doi:10.1002/path.1080
7. Godefroy E, Bhardwaj N. Dysregulation of anti-tumor immunity by the matrix metalloproteinase-2. *Oncoimmunology*. Jan 1 2012;1(1):109-111. doi:10.4161/onci.1.1.17994
8. Godefroy E, et al. Matrix metalloproteinase-2 conditions human dendritic cells to prime inflammatory T(H)2 cells via an IL-12- and OX40L-dependent pathway. *Cancer Cell*. Mar 8 2011;19(3):333-46. doi:10.1016/j.ccr.2011.01.037
9. Godefroy E, et al. alpha v beta3-dependent cross-presentation of matrix metalloproteinase-2 by melanoma cells gives rise to a new tumor antigen. *J Exp Med*. Jul 4 2005;202(1):61-72. doi:10.1084/jem.20042138
10. Shay G, et al. Moving targets: Emerging roles for MMPs in cancer progression and metastasis. *Matrix Biol*. May-Jul 2015;44-46:200-6. doi:10.1016/j.matbio.2015.01.019
11. Houghton AM, et al. Macrophage elastase kills bacteria within murine macrophages. *Nature*. Jul 30 2009;460(7255):637-41. doi:10.1038/nature08181
12. Shimizu-Hirota R, et al. MT1-MMP regulates the PI3Kdelta.Mi-2/NuRD-dependent control of macrophage immune function. *Genes Dev*. Feb 15 2012;26(4):395-413. doi:10.1101/gad.178749.111
13. Godefroy E, et al. Activation of toll-like receptor-2 by endogenous matrix metalloproteinase-2 modulates dendritic-cell-mediated inflammatory responses. *Cell Rep*. Dec 11 2014;9(5):1856-1870. doi:10.1016/j.celrep.2014.10.067
14. Huang B, et al. TLR signaling by tumor and immune cells: a double-edged sword. *Oncogene*. Jan 7 2008;27(2):218-24. doi:10.1038/sj.onc.1210904
15. Urban-Wojciuk Z, et al. The Role of TLRs in Anti-cancer Immunity and Tumor Rejection. *Front Immunol*. 2019;10:2388. doi:10.3389/fimmu.2019.02388
16. Dajon M, et al. Toll-like receptor stimulation in cancer: A pro- and anti-tumor double-edged sword. *Immunobiology*. Jan 2017;222(1):89-100. doi:10.1016/j.imbio.2016.06.009
17. Cen X, et al. The Role of Toll-Like Receptor in Inflammation and Tumor Immunity. *Front Pharmacol*. 2018;9:878. doi:10.3389/fphar.2018.00878
18. Braunstein MJ, et al. Targeting Toll-Like Receptors for Cancer Therapy. *Target Oncol*. Oct 2018;13(5):583-598. doi:10.1007/s11523-018-0589-7
19. Park JS, et al. Involvement of toll-like receptors 2 and 4 in cellular activation by high mobility group box 1 protein. *J Biol Chem*. Feb 27 2004;279(9):7370-7. doi:10.1074/jbc.M306793200
20. Smiley ST, et al. Fibrinogen stimulates macrophage chemokine secretion through toll-like receptor 4. *J Immunol*. Sep 1 2001;167(5):2887-94. doi:10.4049/jimmunol.167.5.2887

21. Biragyn A, et al. Toll-like receptor 4-dependent activation of dendritic cells by beta-defensin 2. *Science*. Nov 1 2002;298(5595):1025-9. doi:10.1126/science.1075565
22. Guillot L, et al. Cutting edge: the immunostimulatory activity of the lung surfactant protein-A involves Toll-like receptor 4. *J Immunol*. Jun 15 2002;168(12):5989-92. doi:10.4049/jimmunol.168.12.5989
23. Termeer C, et al. Oligosaccharides of Hyaluronan activate dendritic cells via toll-like receptor 4. *J Exp Med*. Jan 7 2002;195(1):99-111. doi:10.1084/jem.20001858
24. Okamura Y, et al. The extra domain A of fibronectin activates Toll-like receptor 4. *J Biol Chem*. Mar 30 2001;276(13):10229-33. doi:10.1074/jbc.M100099200
25. Kim S, et al. Carcinoma-produced factors activate myeloid cells through TLR2 to stimulate metastasis. *Nature*. Jan 1 2009;457(7225):102-6. doi:10.1038/nature07623
26. Tang M, et al. Toll-like Receptor 2 Activation Promotes Tumor Dendritic Cell Dysfunction by Regulating IL-6 and IL-10 Receptor Signaling. *Cell Rep*. Dec 29 2015;13(12):2851-64. doi:10.1016/j.celrep.2015.11.053
27. Yang HZ, et al. Blocking TLR2 activity attenuates pulmonary metastases of tumor. *PLoS One*. Aug 5 2009;4(8):e6520. doi:10.1371/journal.pone.0006520
28. Huang B, et al. Toll-like receptors on tumor cells facilitate evasion of immune surveillance. *Cancer Res*. Jun 15 2005;65(12):5009-14. doi:10.1158/0008-5472.CAN-05-0784
29. Yan J, et al. Simultaneous TLR2 inhibition and TLR9 activation synergistically suppress tumor metastasis in mice. *Acta Pharmacol Sin*. Apr 2012;33(4):503-12. doi:10.1038/aps.2011.193
30. Egeblad M, Werb Z. New functions for the matrix metalloproteinases in cancer progression. *Nat Rev Cancer*. Mar 2002;2(3):161-74. doi:10.1038/nrc745
31. Whittaker M, et al. Design and therapeutic application of matrix metalloproteinase inhibitors. *Chem Rev*. Sep 8 1999;99(9):2735-76. doi:10.1021/cr9804543
32. Coussens LM, et al. Matrix metalloproteinase inhibitors and cancer: trials and tribulations. *Science*. Mar 29 2002;295(5564):2387-92. doi:10.1126/science.1067100
33. Dufour A, Overall CM. Missing the target: matrix metalloproteinase antitargets in inflammation and cancer. *Trends Pharmacol Sci*. Apr 2013;34(4):233-42. doi:10.1016/j.tips.2013.02.004
34. Beyersdorf N, et al. Characterization of mouse CD4 T cell subsets defined by expression of KLRG1. *Eur J Immunol*. Dec 2007;37(12):3445-54. doi:10.1002/eji.200737126
35. Bonnefoy N, et al. CD39: A complementary target to immune checkpoints to counteract tumor-mediated immunosuppression. *Oncoimmunology*. May 2015;4(5):e1003015. doi:10.1080/2162402X.2014.1003015
36. Oh DY, et al. Intratumoral CD4(+) T Cells Mediate Anti-tumor Cytotoxicity in Human Bladder Cancer. *Cell*. Jun 3 2020;doi:10.1016/j.cell.2020.05.017
37. Lin H, et al. Host expression of PD-L1 determines efficacy of PD-L1 pathway blockade-mediated tumor regression. *J Clin Invest*. Feb 1 2018;128(2):805-815. doi:10.1172/JCI96113
38. Gros A, et al. PD-1 identifies the patient-specific CD8(+) tumor-reactive repertoire infiltrating human tumors. *J Clin Invest*. May 2014;124(5):2246-59. doi:10.1172/JCI73639
39. Fourcade J, et al. Upregulation of Tim-3 and PD-1 expression is associated with tumor antigen-specific CD8+ T cell dysfunction in melanoma patients. *J Exp Med*. Sep 27 2010;207(10):2175-86. doi:10.1084/jem.20100637
40. Duhen T, et al. Co-expression of CD39 and CD103 identifies tumor-reactive CD8 T cells in human solid tumors. *Nat Commun*. Jul 13 2018;9(1):2724. doi:10.1038/s41467-018-05072-0
41. Noble A, et al. Deficient Resident Memory T Cell and CD8 T Cell Response to Commensals in Inflammatory Bowel Disease. *J Crohns Colitis*. May 21 2020;14(4):525-537. doi:10.1093/ecco-jcc/jjz175
42. Allard B, et al. The ectonucleotidases CD39 and CD73: Novel checkpoint inhibitor targets. *Immunol Rev*. Mar 2017;276(1):121-144. doi:10.1111/imr.12528

43. Gupta PK, et al. CD39 Expression Identifies Terminally Exhausted CD8+ T Cells. *PLoS Pathog*. Oct 2015;11(10):e1005177. doi:10.1371/journal.ppat.1005177
44. McLane LM, et al. CD8 T Cell Exhaustion During Chronic Viral Infection and Cancer. *Annual Review of Immunology*. 2019;37(1):457-495. doi:10.1146/annurev-immunol-041015-055318
45. Ronchetti S, et al. CD8+ T cells: GITR matters. *ScientificWorldJournal*. 2012;2012:308265. doi:10.1100/2012/308265
46. Suvas S, et al. In vivo kinetics of GITR and GITR ligand expression and their functional significance in regulating viral immunopathology. *J Virol*. Sep 2005;79(18):11935-42. doi:10.1128/JVI.79.18.11935-11942.2005
47. Snell LM, et al. CD8 T cell-intrinsic GITR is required for T cell clonal expansion and mouse survival following severe influenza infection. *J Immunol*. Dec 15 2010;185(12):7223-34. doi:10.4049/jimmunol.1001912
48. Peng H, et al. CD62L is critical for maturation and accumulation of murine hepatic NK cells in response to viral infection. *J Immunol*. Apr 15 2013;190(8):4255-62. doi:10.4049/jimmunol.1202395
49. Juelke K, et al. CD62L expression identifies a unique subset of polyfunctional CD56dim NK cells. *Blood*. Aug 26 2010;116(8):1299-307. doi:10.1182/blood-2009-11-253286
50. Djenidi F, et al. CD8+CD103+ tumor-infiltrating lymphocytes are tumor-specific tissue-resident memory T cells and a prognostic factor for survival in lung cancer patients. *J Immunol*. Apr 1 2015;194(7):3475-86. doi:10.4049/jimmunol.1402711
51. Ganesan AP, et al. Tissue-resident memory features are linked to the magnitude of cytotoxic T cell responses in human lung cancer. *Nat Immunol*. Aug 2017;18(8):940-950. doi:10.1038/ni.3775
52. Amsen D, et al. Tissue-resident memory T cells at the center of immunity to solid tumors. *Nat Immunol*. Jun 2018;19(6):538-546. doi:10.1038/s41590-018-0114-2
53. Mami-Chouaib F, et al. Resident memory T cells, critical components in tumor immunology. *J Immunother Cancer*. Sep 4 2018;6(1):87. doi:10.1186/s40425-018-0399-6
54. DeLong JH, et al. Cytokine- and TCR-Mediated Regulation of T Cell Expression of Ly6C and Sca-1. *J Immunol*. Mar 1 2018;200(5):1761-1770. doi:10.4049/jimmunol.1701154
55. Wu K, et al. CD4(+) TSCMs in the Bone Marrow Assist in Maturation of Antibodies against Influenza in Mice. *Mediators Inflamm*. 2019;2019:3231696. doi:10.1155/2019/3231696
56. Hildner K, et al. Batf3 deficiency reveals a critical role for CD8alpha+ dendritic cells in cytotoxic T cell immunity. *Science*. Nov 14 2008;322(5904):1097-100. doi:10.1126/science.1164206
57. Edwards AD, et al. Toll-like receptor expression in murine DC subsets: lack of TLR7 expression by CD8 alpha+ DC correlates with unresponsiveness to imidazoquinolines. *Eur J Immunol*. Apr 2003;33(4):827-33. doi:10.1002/eji.200323797
58. Shinkai Y, et al. RAG-2-deficient mice lack mature lymphocytes owing to inability to initiate V(D)J rearrangement. *Cell*. Mar 6 1992;68(5):855-67. doi:10.1016/0092-8674(92)90029-c
59. Aspord C, et al. Plasmacytoid dendritic cells support melanoma progression by promoting Th2 and regulatory immunity through OX40L and ICOSL. *Cancer Immunol Res*. Dec 2013;1(6):402-15. doi:10.1158/2326-6066.CIR-13-0114-T
60. Lauerova L, et al. Malignant melanoma associates with Th1/Th2 imbalance that coincides with disease progression and immunotherapy response. *Neoplasma*. 2002;49(3):159-66.
61. Vasselon T, et al. TLR2 recognizes a bacterial lipopeptide through direct binding. *J Immunol*. Dec 15 2004;173(12):7401-5. doi:10.4049/jimmunol.173.12.7401

62. Lee HK, et al. Cytoplasmic domain-mediated dimerizations of toll-like receptor 4 observed by beta-lactamase enzyme fragment complementation. *J Biol Chem*. Mar 12 2004;279(11):10564-74. doi:10.1074/jbc.M311564200
63. Wang YC, et al. Toll-like receptor 2/4 heterodimer mediates inflammatory injury in intracerebral hemorrhage. *Ann Neurol*. Jun 2014;75(6):876-89. doi:10.1002/ana.24159
64. Good DW, et al. Toll-like receptor 2 is required for LPS-induced Toll-like receptor 4 signaling and inhibition of ion transport in renal thick ascending limb. *J Biol Chem*. Jun 8 2012;287(24):20208-20. doi:10.1074/jbc.M111.336255
65. Shimoda M, Khokha R. Metalloproteinases in extracellular vesicles. *Biochim Biophys Acta Mol Cell Res*. Nov 2017;1864(11 Pt A):1989-2000. doi:10.1016/j.bbamcr.2017.05.027
66. Han KY, et al. Evidence for the Involvement of MMP14 in MMP2 Processing and Recruitment in Exosomes of Corneal Fibroblasts. *Invest Ophthalmol Vis Sci*. Aug 2015;56(9):5323-9. doi:10.1167/iovs.14-14417
67. Zucker S, et al. Metastatic mouse melanoma cells release collagen-gelatin degrading metalloproteinases as components of shed membrane vesicles. *Biochim Biophys Acta*. Apr 16 1987;924(1):225-37. doi:10.1016/0304-4165(87)90091-2
68. Zanoni I, et al. CD14 controls the LPS-induced endocytosis of Toll-like receptor 4. *Cell*. Nov 11 2011;147(4):868-80. doi:10.1016/j.cell.2011.09.051
69. Tan Y, et al. Mechanisms of Toll-like Receptor 4 Endocytosis Reveal a Common Immune-Evasion Strategy Used by Pathogenic and Commensal Bacteria. *Immunity*. Nov 17 2015;43(5):909-22. doi:10.1016/j.immuni.2015.10.008
70. Dietrich N, et al. Murine toll-like receptor 2 activation induces type I interferon responses from endolysosomal compartments. *PLoS One*. Apr 20 2010;5(4):e10250. doi:10.1371/journal.pone.0010250
71. Stack J, et al. TRAM is required for TLR2 endosomal signaling to type I IFN induction. *J Immunol*. Dec 15 2014;193(12):6090-102. doi:10.4049/jimmunol.1401605
72. Brandt KJ, et al. TLR2 ligands induce NF-kappaB activation from endosomal compartments of human monocytes. *PLoS One*. 2013;8(12):e80743. doi:10.1371/journal.pone.0080743
73. Chow AK, et al. Caveolin-1 inhibits matrix metalloproteinase-2 activity in the heart. *J Mol Cell Cardiol*. Apr 2007;42(4):896-901. doi:10.1016/j.yjmcc.2007.01.008
74. Jobin PG, et al. New intracellular activities of matrix metalloproteinases shine in the moonlight. *Biochim Biophys Acta Mol Cell Res*. Nov 2017;1864(11 Pt A):2043-2055. doi:10.1016/j.bbamcr.2017.05.013
75. Yang Z, et al. Extracellular matrix metalloproteinase 2 levels are regulated by the low density lipoprotein-related scavenger receptor and thrombospondin 2. *J Biol Chem*. Mar 16 2001;276(11):8403-8. doi:10.1074/jbc.M008925200
76. Emonard H, et al. Low density lipoprotein receptor-related protein mediates endocytic clearance of pro-MMP-2.TIMP-2 complex through a thrombospondin-independent mechanism. *J Biol Chem*. Dec 24 2004;279(52):54944-51. doi:10.1074/jbc.M406792200
77. Johanns M, et al. Cellular uptake of proMMP-2:TIMP-2 complexes by the endocytic receptor megalin/LRP-2. *Sci Rep*. Jun 28 2017;7(1):4328. doi:10.1038/s41598-017-04648-y
78. Dufour A, et al. Role of the hemopexin domain of matrix metalloproteinases in cell migration. *J Cell Physiol*. Dec 2008;217(3):643-51. doi:10.1002/jcp.21535
79. Farnebo L, et al. Targeting Toll-like receptor 2 inhibits growth of head and neck squamous cell carcinoma. *Oncotarget*. Apr 30 2015;6(12):9897-907. doi:10.18632/oncotarget.3393
80. Littlepage LE, et al. Matrix metalloproteinases contribute distinct roles in neuroendocrine prostate carcinogenesis, metastasis, and angiogenesis progression. *Cancer Res*. Mar 15 2010;70(6):2224-34. doi:10.1158/0008-5472.CAN-09-3515

81. Astarita JL, et al. Podoplanin: emerging functions in development, the immune system, and cancer. *Front Immunol*. 2012;3:283. doi:10.3389/fimmu.2012.00283
82. Bussard KM, et al. Tumor-associated stromal cells as key contributors to the tumor microenvironment. *Breast Cancer Res*. Aug 11 2016;18(1):84. doi:10.1186/s13058-016-0740-2
83. Noubade R, et al. Beyond cDC1: Emerging Roles of DC Crosstalk in Cancer Immunity. *Front Immunol*. 2019;10:1014. doi:10.3389/fimmu.2019.01014
84. Binnewies M, et al. Unleashing Type-2 Dendritic Cells to Drive Protective Antitumor CD4(+) T Cell Immunity. *Cell*. Apr 18 2019;177(3):556-571 e16. doi:10.1016/j.cell.2019.02.005
85. Ruhland MK, et al. Visualizing Synaptic Transfer of Tumor Antigens among Dendritic Cells. *Cancer Cell*. Jun 8 2020;37(6):786-799 e5. doi:10.1016/j.ccell.2020.05.002
86. Balan S, Bhardwaj N. Cross-Presentation of Tumor Antigens Is Ruled by Synaptic Transfer of Vesicles among Dendritic Cell Subsets. *Cancer Cell*. Jun 8 2020;37(6):751-753. doi:10.1016/j.ccell.2020.05.013
87. Seillet C, et al. CD8alpha+ DCs can be induced in the absence of transcription factors Id2, Nfil3, and Batf3. *Blood*. Feb 28 2013;121(9):1574-83. doi:10.1182/blood-2012-07-445650
88. Mott KR, et al. Batf3 deficiency is not critical for the generation of CD8alpha(+) dendritic cells. *Immunobiology*. Apr 2015;220(4):518-24. doi:10.1016/j.imbio.2014.10.019
89. Theisen DJ, Murphy KM. WDFY4 is required for cross-presentation in response to viral and tumor antigens.pdf>. *Science*. 2018:694-699.
90. Hofmann UB, et al. Matrix metalloproteinases in human melanoma cell lines and xenografts: increased expression of activated matrix metalloproteinase-2 (MMP-2) correlates with melanoma progression. *Br J Cancer*. Nov 1999;81(5):774-82. doi:10.1038/sj.bjc.6690763
91. Kurschat P, et al. Tissue inhibitor of matrix metalloproteinase-2 regulates matrix metalloproteinase-2 activation by modulation of membrane-type 1 matrix metalloproteinase activity in high and low invasive melanoma cell lines. *J Biol Chem*. Jul 23 1999;274(30):21056-62. doi:10.1074/jbc.274.30.21056
92. Li YC, et al. Circulating tumor cells promote the metastatic colonization of disseminated carcinoma cells by inducing systemic inflammation. *Oncotarget*. Apr 25 2017;8(17):28418-28430. doi:10.18632/oncotarget.16084
93. Lu Y, et al. TLR4 plays a crucial role in MSC-induced inhibition of NK cell function. *Biochem Biophys Res Commun*. Aug 21 2015;464(2):541-7. doi:10.1016/j.bbrc.2015.07.002
94. Tanne A, et al. Distinguishing the immunostimulatory properties of noncoding RNAs expressed in cancer cells. *Proc Natl Acad Sci U S A*. Dec 8 2015;112(49):15154-9. doi:10.1073/pnas.1517584112
95. Blasi E, et al. Selective immortalization of murine macrophages from fresh bone marrow by a raf/myc recombinant murine retrovirus. *Nature*. Dec 19-1986 Jan 1 1985;318(6047):667-70. doi:10.1038/318667a0
96. Atianand MK, Fitzgerald KA. Molecular basis of DNA recognition in the immune system. *J Immunol*. Mar 1 2013;190(5):1911-8. doi:10.4049/jimmunol.1203162
97. Pfeifer A, et al. Suppression of angiogenesis by lentiviral delivery of PEX, a noncatalytic fragment of matrix metalloproteinase 2. *Proc Natl Acad Sci U S A*. Oct 24 2000;97(22):12227-32. doi:10.1073/pnas.220399597

MAIN FIGURES

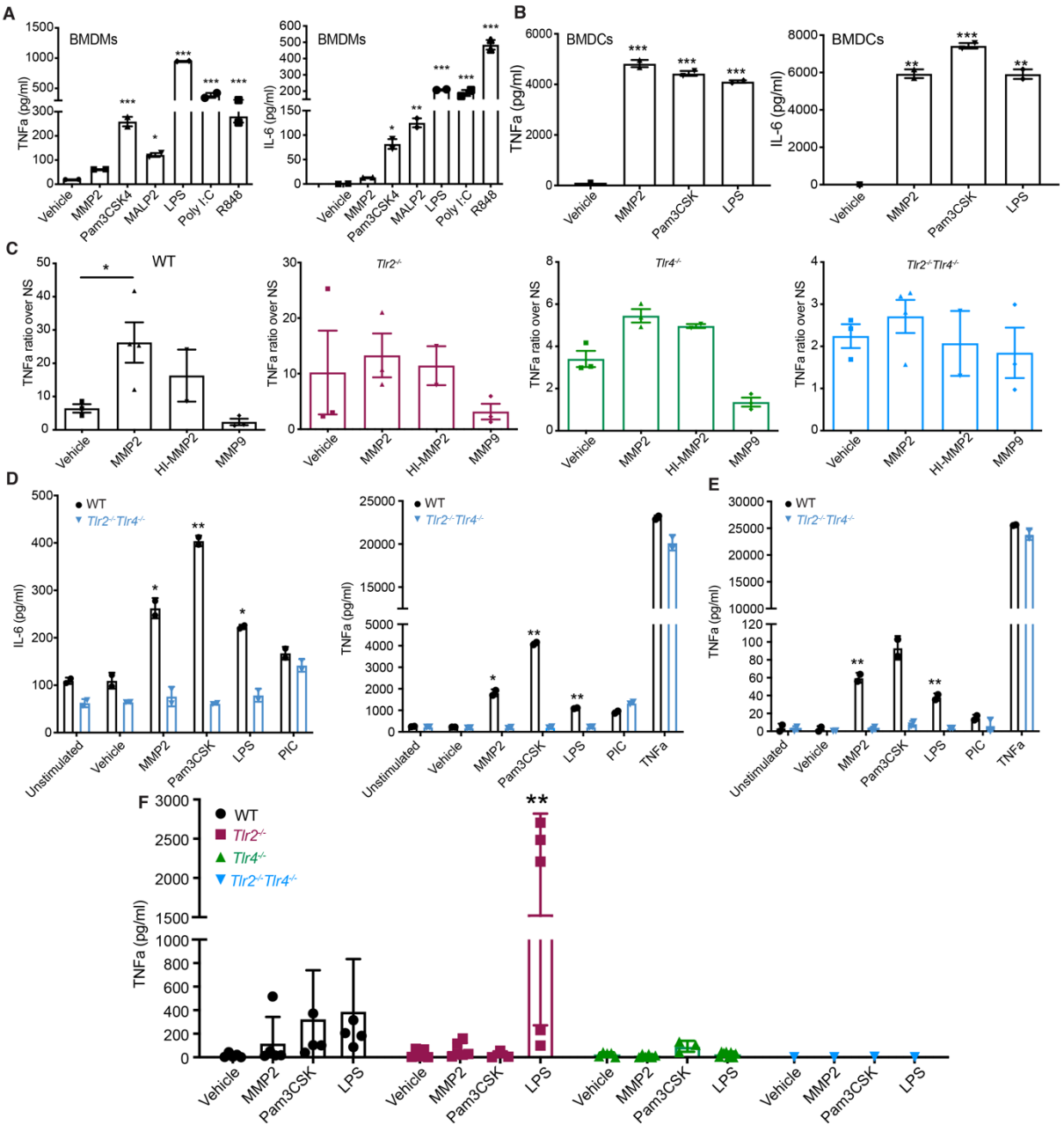

Figure 1. MMP2 signaling is mediated by TLR2 and TLR4: Pro-inflammatory cytokine secretion by primary APCs and immortalized APC cell lines. Briefly, cells were stimulated with MMP2, MMP9, vehicle control or TLR agonists overnight. All stimulations were performed with $2x10^5$ cells per condition in 200µl volume. 16-18 hours post stimulation, supernatants were collected and

cytometric bead array (CBA) for mouse inflammatory cytokines was performed. A-B. BMDMs (A) and BMDCs (B) responded to stimulation and secreted TNFα and IL-6. N=2. Data is representative of 2 independent experiments with mean ± SEM. *p<0.05, **p<0.01 and ***p<0.001. One-way ANOVA with Dunnet's post hoc test. C. TNFα secretion by Im-MACS from WT and Tlr-deficient mice. Each graph represents the ratio over unstimulated cells. N=2-4. Data is representative of 4 independent experiments with mean ± SEM. *p<0.05. One-way ANOVA with Dunnet's post hoc test. D-E. TNFα and IL-6 secretion by primary $CD11c^{+}$ DCs isolated from lung (D) and spleen (E). N=2. Data representative of 2 experiments. Mean ± SEM. *p<0.05, **p<0.01 and ***p<0.001 versus *Tlr2*$^{-/-}$*Tlr4*$^{-/-}$ cells. Multiple unpaired T-test with using Holm-Sidak correction for multiple comparisons. F. TNFα secretion in serum of WT, *Tlr2*$^{-/-}$, *Tlr4*$^{-/-}$ and *Tlr2*$^{-/-}$ *Tlr4*$^{-/-}$ mice 3 hours post i.v. injection with Vehicle, MMP2, Pam3CSK4 and LPS. Data is representative of 4 independent experiments with mean ± SEM. *p<0.05, **p<0.01 and ***p<0.001. Two-way ANOVA with Dunnet's post hoc test.

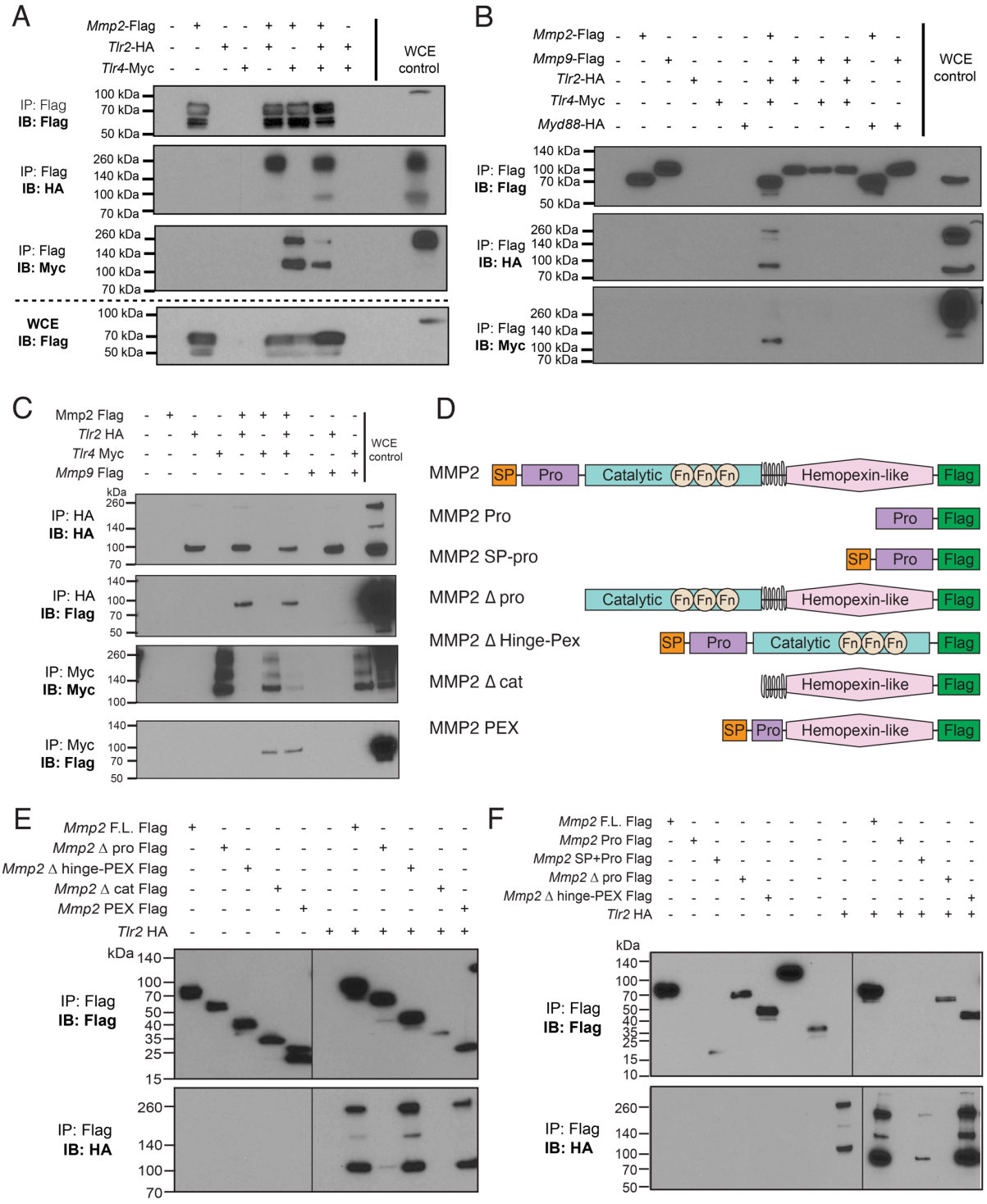

Figure 2. MMP2 binds and precipitates with TLR2 and TLR4: A-B. HEK293T co-transfection followed by Flag pull-down using magnetic beads. *Mmp2*-Flag was co-transfected with *Tlr2*-HA, *Tlr4*-Myc or both plasmids (A). *Mmp9*-Flag co-transfection with Tlr-plasmids or *Myd88*-HA plasmid

was also evaluated (B). C. Reverse co-IP of *Mmp2*-Flag or *Mmp9*-Flag co-transfected with *Tlr2*-HA, *Tlr4*-Myc or both plasmids. HA or Myc pull down using anti-HA agarose or Anti-c-MYC agarose beads. D. Schematic of the different MMP2 constructs used in the co-IP to identify the binding domain. E-F. Different MMP2 domains were deleted or expressed alone and tested for co-IP with *Tlr2*-HA. Black line indicates where membrane ends/was cut. All transfections were performed using Lipofectamine 3000 and protein was extracted 20-24 hours post-transfection. IP = immunoprecipitation; IB = immunoblotting; WCE = whole cell extract; Δ = deletion.

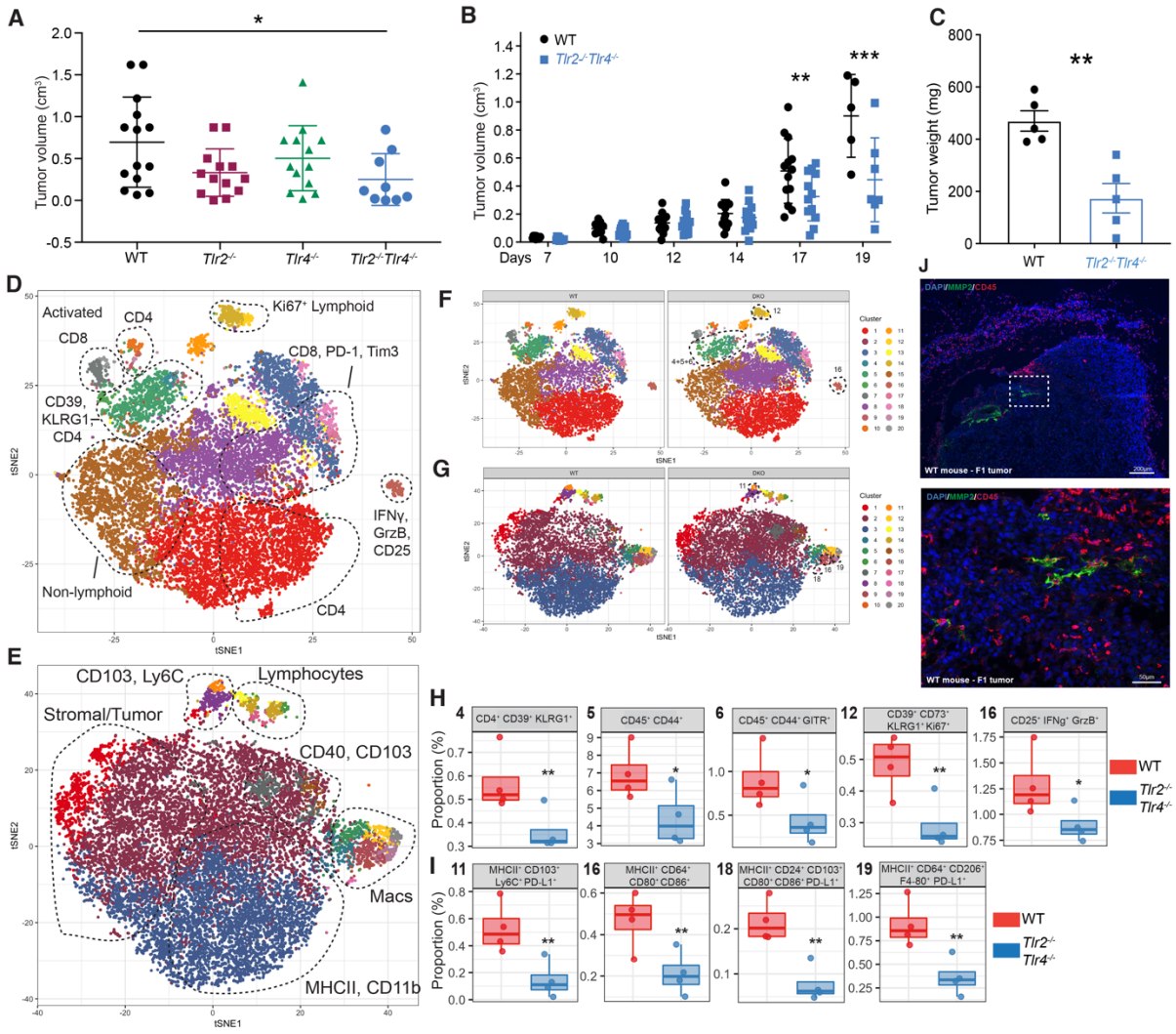

Figure 3. Smaller tumor growth and differential tumor microenvironment in *Tlr2*$^{-/-}$*Tlr4*$^{-/-}$ mice: 3x10^5 B16 F1 cells were injected sub-cutaneously into WT or *Tlr* deficient mice and tumors were analyzed 15-19 days later. A. Tumor volume in WT, *Tlr2*$^{-/-}$, *Tlr4*$^{-/-}$ and *Tlr2*$^{-/-}$*Tlr4*$^{-/-}$ mice at day 15. Data is representative of 4 independent experiments with mean ± SEM. *p<0.05. Two-way ANOVA with Dunnet's post hoc test. B. Tumor growth kinetics between WT and *Tlr2*$^{-/-}$*Tlr4*$^{-/-}$ mice during the course of 19 days. C. Tumor weight (mg) at day 18-19. A-C. Data is representative of 5 independent experiments with mean ± SEM. **p<0.01 and ***p<0.001.Two-way ANOVA with Sidak's correction for multiple comparisons. D-I. CyTOF analysis of lymphoid and myeloid panels in the TME at day 19 between WT and *Tlr2*$^{-/-}$*Tlr4*$^{-/-}$ mice. viSNE plot of immune, stromal and tumor

cell clusters present in the lymphoid panel (D) and myeloid panel (E). Comparison between WT and *Tlr2*$^{-/-}$*Tlr4*$^{-/-}$ mice in the lymphoid (F) and myeloid (G) panel, highlighting differentially expressed clusters (dotted lines). Statistically significant clusters from the lymphoid panel (H) and myeloid panel (I) are identified. Data is representative of 2-4 mice with mean ±SEM. *p<0.05, **p<0.01 and ***p<0.001. p values were adjusted using FDR. Statistical analysis was performed using binomial generalized linear mixed-effects model (GLMM). J. IF staining of MMP2 (green), CD45 (red) and DAPI (blue).

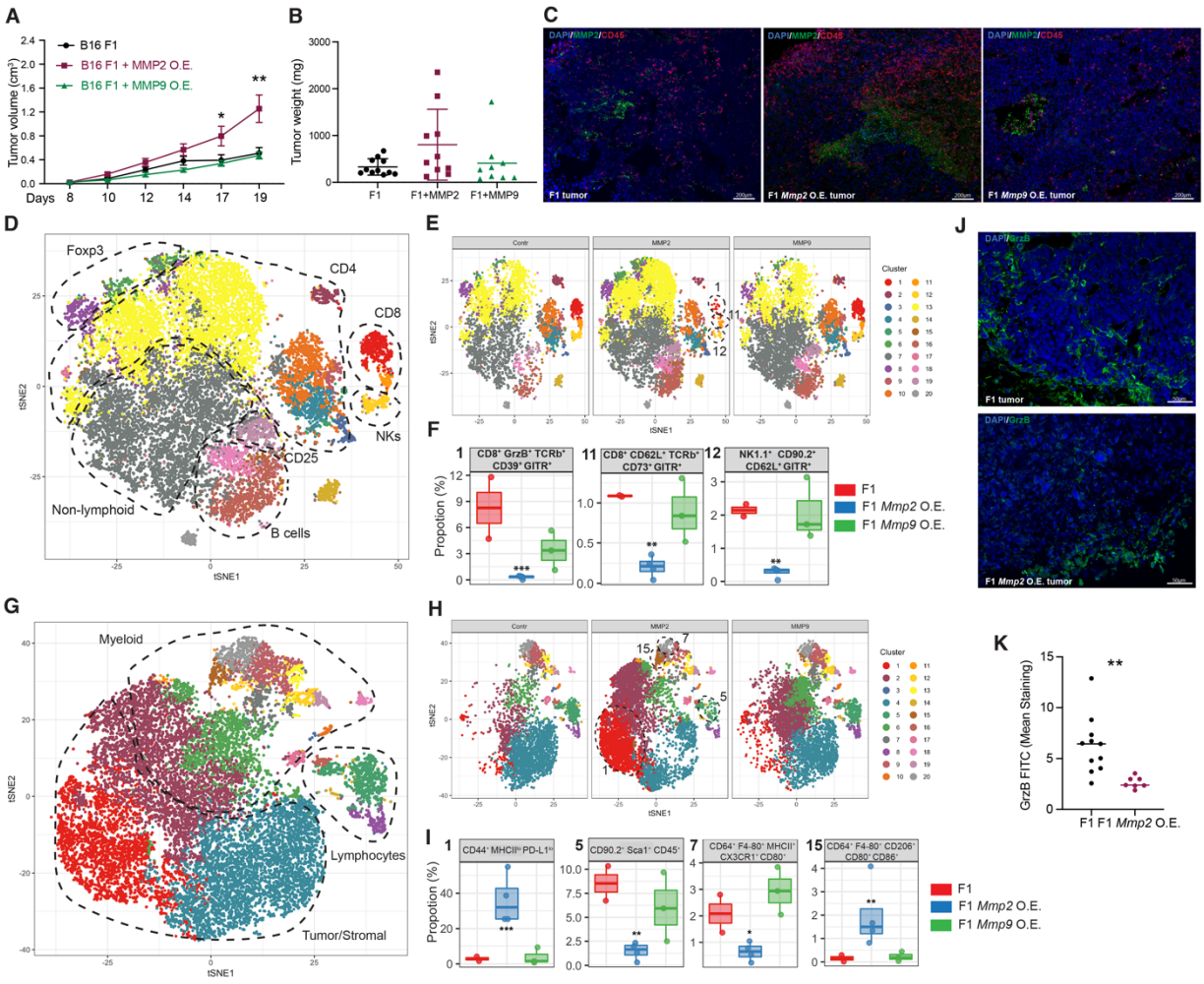

Figure 4. *Mmp2* overexpression in B16 cells promotes melanoma tumor growth: *Mmp2* and *Mmp9* were overexpressed (O.E.) in B16 F1 cells and injected into mice. A-B. Tumor kinetics was measured up to 20 days. Tumor volume (A) and weight (B) are displayed. N=8-10 mice per group. Data is representative of 5 independent experiments with mean ± SEM. *p<0.05, **p<0.01 and ***p<0.001. Two-way ANOVA with Dunnet's post hoc test. C. Immunofluorescence (IF) staining for MMP2 (green), CD45 (red) and DAPI (blue). Scale bars: D-F. CyTOF analysis of Lymphoid panel. viSNE plot of immune, stromal and tumor cell clusters present in the tumors at day 19 (D) identified with aid of single marker expression in all samples. Population comparison between F1 and F1 *Mmp* OE tumors (E) were identified and clusters differentially expressed between the different groups of tumors were identified (F). G-I. CyTOF analysis of Myeloid panel. viSNE plot

of immune, stromal and tumor cell clusters present in the tumors at day 19 (G) identified with aid of single marker expression in all samples. Population comparison between F1 and F1 MMP OE tumors (H) were identified and clusters differentially expressed between the different groups of tumors were identified (I). Data is representative of 2-4 mice with mean ±SEM. *p<0.05, **p<0.01 and ***p<0.001. p values were adjusted using FDR. Statistical analysis was performed using binomial generalized linear mixed-effects model (GLMM). J. IF of Granzyme-B (green) and DAPI (blue) in F1 tumors (top) and F1 *Mmp2* OE tumors (bottom). K. Quantification of GrzB staining. N=8-12 sections with mean ±SEM. **p<0.01. Student t-test.

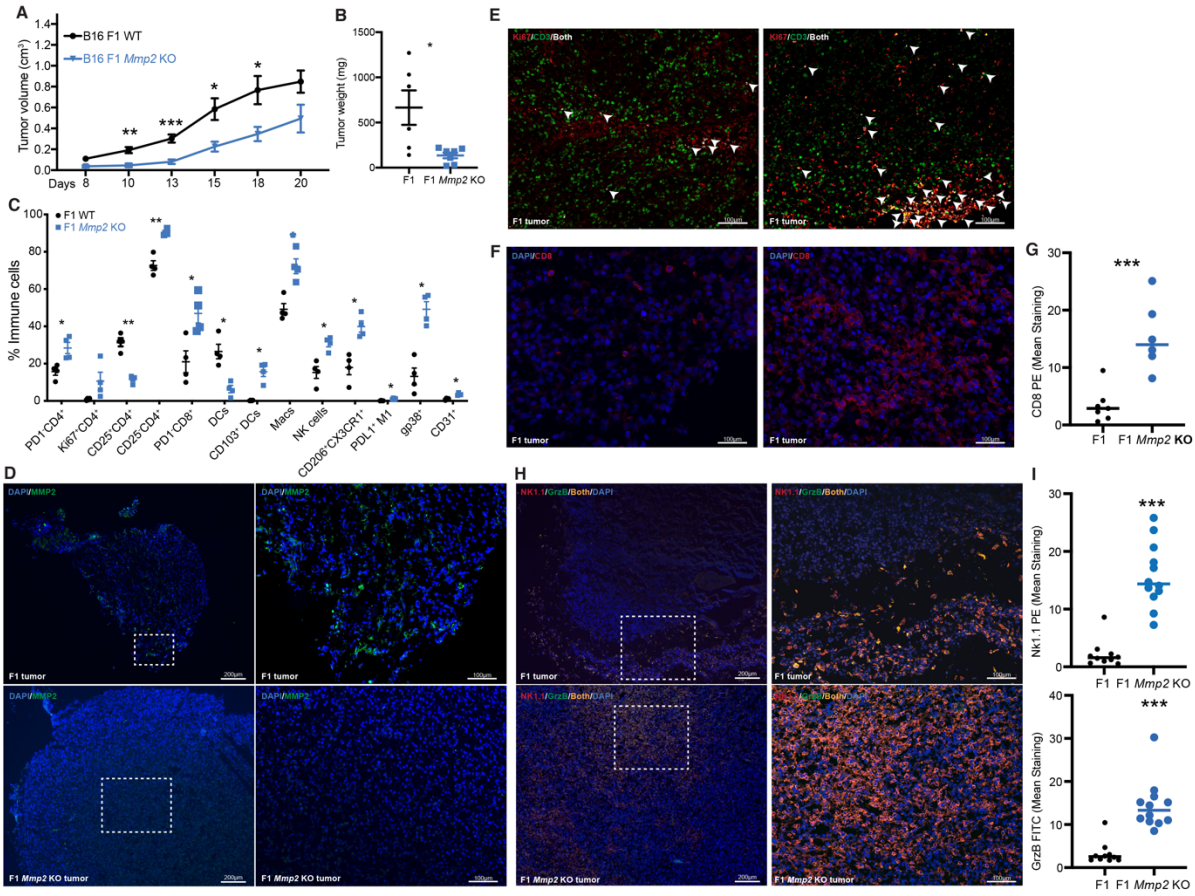

Figure 5. *Mmp2* depletion in B16 cells impairs melanoma tumor growth: The levels of *Mmp2* in the B16 was modulated by CRISPR knock-out systems. $3x10^5$ B16 F1 or F1 *Mmp2* KO cells and tumors were measured up to 20 days. Tumor volume (A) and weight (B) are displayed. Data is representative of 5 independent experiments with mean ± SEM. N=8-10 mice per group. *p<0.05, **p<0.01 and ***p<0.001. Multiple t-tests with Holm-Sidak correction for multiple comparisons. C. FACS analysis on day 19 shows changes in hematopoietic cell infiltration. Data is representative of 3 independent experiments with mean ± SEM. N=4 mice per group. *p<0.05, **p<0.01 and ***p<0.001. Multiple t-tests with Holm-Sidak correction for multiple comparisons. D-I. Immunofluorescence (IF) stainings. D. IF staining for MMP2 (green) and DAPI (blue). F1 control tumors on the top panel and F1 *Mmp2* KO controls on the bottom panel. E. IF colocalization (white) of $CD3^+$ T cells (green) with Ki67 (red) in *Mmp2* KO tumors. Colocalization is shown is

white arrowheads. F. IF staining of CD8 (red) and DAPI (blue). G. Quantification of the CD8 staining. Data representative of 2 experiments, N=6, mean± SEM. ***p<0.001. Student t-test. H. IF staining of NK1.1 (red), Granzyme B (green) and DAPI (blue) infiltrates in the tumor bed. F1 tumors on top panels and F1 *Mmp2* KO tumors on the bottom panels. Colocalization is shown in orange. I. Quantification of NK1.1 and Granzyme-B staining. Data representative of 2 experiments, N=6, mean± SEM ***p<0.001. Student t-test.

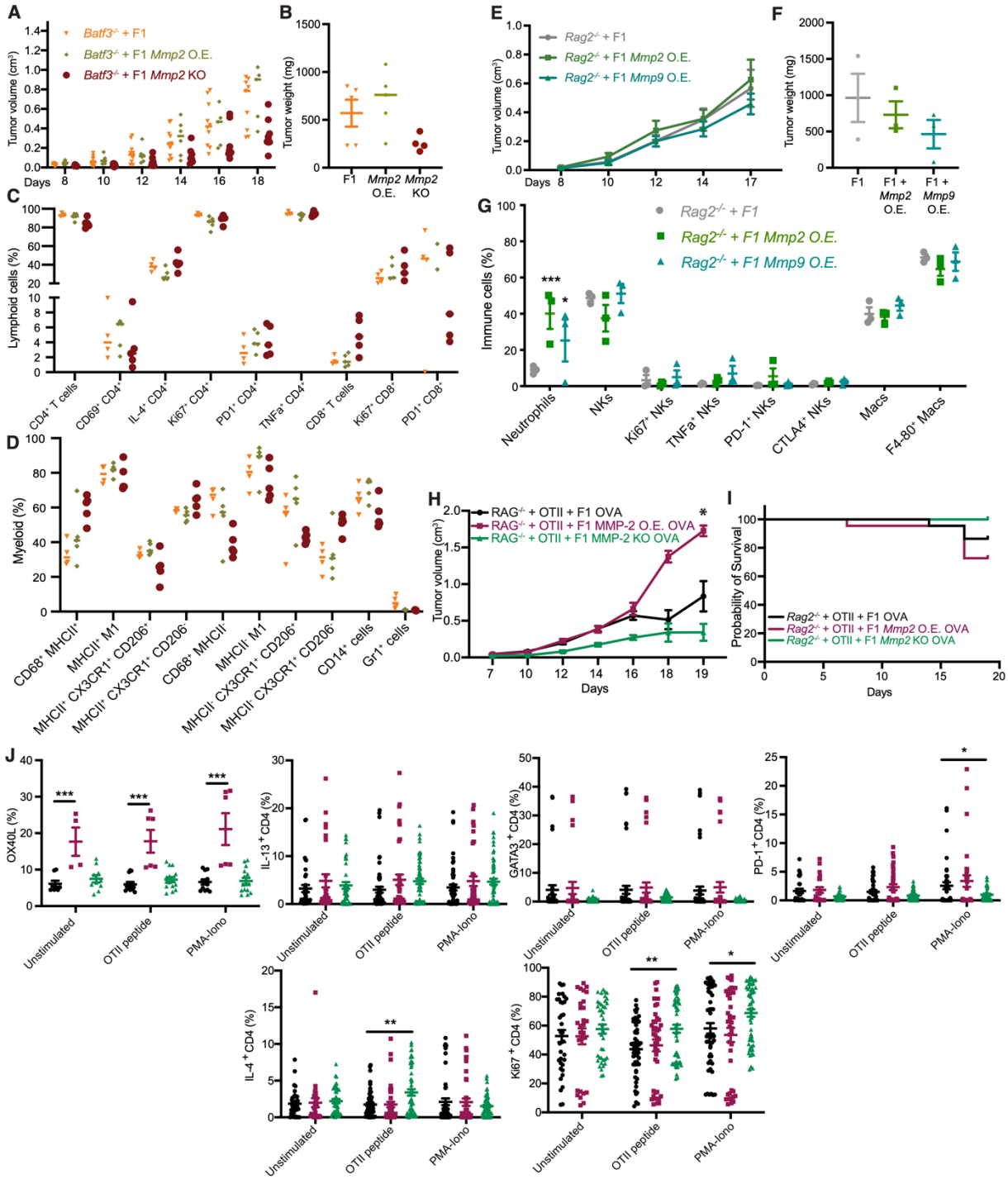

Figure 6. MMP2 signaling in B16 TME involves BATF3 DCs and lymphoid cells: The role of lymphoid cells and BATF3 DCs was evaluated by using *Rag2*$^{-/-}$and *Batf3*$^{-/-}$ mice, respectively. Mice were subcutaneously injected with 3x10^5 B16 F1, F1 *Mmp2* OE, *Mmp9* OE or F1 *Mmp2* KO cells and tumors were measured up to 20 days. A-D. Tumor growth comparison in *Batf3*$^{-/-}$ mice.

Tumor volume (A) and weight (B) are displayed. Data is representative of 3 experiments with mean ± SEM and 8-10 mice per group. One-way ANOVA with Dunnet's post hoc test. FACS analysis on day 18 shows changes in hematopoietic cell infiltration for lymphoid (C) and myeloid cells (D). Data is representative of 2 experiments with mean ± SEM and 4 mice per group. Two-way ANOVA with Dunnet's post hoc test. E-F. Tumor growth comparison in *Rag2*$^{-/-}$ mice. Tumor volume (E) and weight (F) are displayed. G. FACS analysis on day 18 shows changes in hematopoietic cell infiltration. Data is representative of 2 experiments with mean ± SEM and 5-7 mice per group. H-I. Tumor growth comparison in *Rag2*$^{-/-}$ mice transferred with OTII cells and B16 OVA O.E. tumors. Tumor volume (H) and survival curve (I) are displayed. J. FACS analysis of ex vivo stimulated CD4^{+} T cells from tumors at day 18. Data is representative of 2 independent experiments with mean ± SEM. N=4-6 mice per group. Student t-test, * is $p<0.05$, ** is $p<0.01$ and *** is $p<0.001$.